REPORT DOCUMENTATION PAGE

Form Approved OMB NO. 0704-0188

1. REPORT DATE (DD-MM-YYYY)	2. REPORT TYPE	3. DATES COVERED (From - To)
17-06-2010	Final Report	1-Oct-2007 - 31-Aug-2009

4. TITLE AND SUBTITLE

A Novel Approach to Chemical Communications (Phase I)

5a. CONTRACT NUMBER
W911NF-07-1-0639

5b. GRANT NUMBER

5c. PROGRAM ELEMENT NUMBER
7620AK

6. AUTHORS

Lawrence S. Bernstein, Frank O. Clark, Irving R. Epstein (PI), Seth Fraden, Darren R. Link, Jordan B. Pollack, Steven Richtsmeier, Anatol M. Zhabotinsky, (deceased 9/16/08)

5d. PROJECT NUMBER

5e. TASK NUMBER

5f. WORK UNIT NUMBER

7. PERFORMING ORGANIZATION NAMES AND ADDRESSES

Brandeis University
415 South Street
MS 116
Waltham, MA 02454 -9110

8. PERFORMING ORGANIZATION REPORT NUMBER

9. SPONSORING/MONITORING AGENCY NAME(S) AND ADDRESS(ES)

U.S. Army Research Office
P.O. Box 12211
Research Triangle Park, NC 27709-2211

10. SPONSOR/MONITOR'S ACRONYM(S)
ARO

11. SPONSOR/MONITOR'S REPORT NUMBER(S)
53390-MS-DRP.1

12. DISTRIBUTION AVAILIBILITY STATEMENT

Approved for Public Release; Distribution Unlimited

13. SUPPLEMENTARY NOTES

The views, opinions and/or findings contained in this report are those of the author(s) and should not contrued as an official Department of the Army position, policy or decision, unless so designated by other documentation.

14. ABSTRACT

The ultimate goal of this project was to develop a device for encoding and sending modulated high frequency optical signals utilizing a novel combination of chemical oscillators, chemiluminescent reactions and microfluidic technology. Our research team consisted of scientists and engineers from Brandeis University, Spectral Sciences, Inc., the Air Force Research Laboratory, Hanscom AFB, and RainDance Technologies, Inc..

We have made significant progress toward this goal and have discovered several potentially significant new

15. SUBJECT TERMS

chemical communications, chemiluminescence, oscillatoing chemical reactions, encoding, programmable simulator

16. SECURITY CLASSIFICATION OF:			17. LIMITATION OF ABSTRACT	15. NUMBER OF PAGES	19a. NAME OF RESPONSIBLE PERSON
a. REPORT	b. ABSTRACT	c. THIS PAGE			Irving Epstein
UU	UU	UU	UU		19b. TELEPHONE NUMBER: 781-736-2503

Report Title

A Novel Approach to Chemical Communications (Phase I)

ABSTRACT

The ultimate goal of this project was to develop a device for encoding and sending modulated high frequency optical signals utilizing a novel combination of chemical oscillators, chemiluminescent reactions and microfluidic technology. Our research team consisted of scientists and engineers from Brandeis University, Spectral Sciences, Inc., the Air Force Research Laboratory, Hanscom AFB, and RainDance Technologies, Inc..

We have made significant progress toward this goal and have discovered several potentially significant new phenomena in the course of our investigations. In particular, we have been able to increase the frequency of the Belousov-Zhabotinsky chemical oscillator by three to four orders of magnitude and have constructed microfluidic circuits to produce one- and two –dimensional arrays of coupled oscillators, which give rise to a variety of patterns that can be used to build communications and computational devices. We have tested two novel approaches for encoding chemical signals, developed a programmable simulator to mimic the signals, and carried out field tests to analyze problems of distinguishing the signal from the background. Mathematical models have been developed and successfully employed to simulate the experimental phenomena. Nonetheless, there remains significant work to be done in order to produce an operable device.

List of papers submitted or published that acknowledge ARO support during this reporting period. List the papers, including journal references, in the following categories:

(a) Papers published in peer-reviewed journals (N/A for none)

M. Toiya, V.K. Vanag and I.R. Epstein, “Diffusively Coupled Chemical Oscillators in a Microfluidic Assembly,” Angew. Chem. Int. Ed. 47, 7753-7755 (2008)

T. Bánsági Jr., M. Leda, M. Toiya, A. M. Zhabotinsky, and I. R. Epstein, “High-frequency oscillations in the Belousov-Zhabotinsky reaction,” J. Phys. Chem. A 113, 5644-5648 (2009)

M. Toiya, H.O. Gonzalez-Ochoa, V. K. Vanag, S. Fraden, and I.R. Epstein, “Synchronous Regimes of Oscillatory Microdroplets,” J. Phys. Chem. Lett. 1, 1241-1246 (2010).

Number of Papers published in peer-reviewed journals: 3.00

(b) Papers published in non-peer-reviewed journals or in conference proceedings (N/A for none)

Number of Papers published in non peer-reviewed journals: 0.00

(c) Presentations

I. Epstein, S. Fraden, J. Pollack, A.M. Zhabotinsky, D. Link, S. Richtsmeier, "Chemical Communications," Infochemistry, Cambridge, MA, Oct. 15-17, 2008

I. Epstein, "Cooperative Behavior of Nano- and Micro-Oscillators," Emergence in Chemical Systems, Anchorage, AK, June 26, 2009

Number of Presentations: 2.00

Non Peer-Reviewed Conference Proceeding publications (other than abstracts):

Number of Non Peer-Reviewed Conference Proceeding publications (other than abstracts): 0

Peer-Reviewed Conference Proceeding publications (other than abstracts):

Number of Peer-Reviewed Conference Proceeding publications (other than abstracts): 0

(d) Manuscripts

Number of Manuscripts: 0.00

Patents Submitted

Patents Awarded

Awards

I.R. Epstein, Honorary Professorship, China University of Mining and Technology, June, 2009

Graduate Students

NAME	PERCENT_SUPPORTED
Marcus Long	0.25
FTE Equivalent:	**0.25**
Total Number:	**1**

Names of Post Doctorates

NAME	PERCENT_SUPPORTED
Masahiro Toiya	0.50
Marcin Leda	1.00
Tamas Bansagi	1.00
FTE Equivalent:	**2.50**
Total Number:	**3**

Names of Faculty Supported

NAME	PERCENT_SUPPORTED	National Academy Member
Irving Epstein	0.25	No
Seth Fraden	0.22	No
Jordan Pollack	0.22	No
Anatol Zhabotinsky	0.75	No
FTE Equivalent:	**1.44**	
Total Number:	**4**	

Names of Under Graduate students supported

NAME	PERCENT_SUPPORTED
FTE Equivalent:	
Total Number:	

Student Metrics

This section only applies to graduating undergraduates supported by this agreement in this reporting period

The number of undergraduates funded by this agreement who graduated during this period:	0.00
The number of undergraduates funded by this agreement who graduated during this period with a degree in science, mathematics, engineering, or technology fields:.....	0.00
The number of undergraduates funded by your agreement who graduated during this period and will continue to pursue a graduate or Ph.D. degree in science, mathematics, engineering, or technology fields:.....	0.00
Number of graduating undergraduates who achieved a 3.5 GPA to 4.0 (4.0 max scale):	0.00
Number of graduating undergraduates funded by a DoD funded Center of Excellence grant for Education, Research and Engineering:	0.00
The number of undergraduates funded by your agreement who graduated during this period and intend to work for the Department of Defense	0.00
The number of undergraduates funded by your agreement who graduated during this period and will receive scholarships or fellowships for further studies in science, mathematics, engineering or technology fields:	0.00

Names of Personnel receiving masters degrees

NAME
Total Number:

Names of personnel receiving PHDs

NAME
Total Number:

Names of other research staff

NAME	PERCENT_SUPPORTED	
Claudia Wellington	0.25	No
FTE Equivalent:	**0.25**	
Total Number:	**1**	

Sub Contractors (DD882)

1 a. Spectral Sciences, Inc.

1 b. 4 Fourth Avenue

Burlington MA 01803-3304

Sub Contractor Numbers (c):

Patent Clause Number (d-1):

Patent Date (d-2):

Work Description (e): Developing programmable simulator, interfacing with Air Force Research Laboratory, conducting fi

Sub Contract Award Date (f-1): 10/1/2007 12:00:00AM

Sub Contract Est Completion Date(f-2): 8/31/2009 12:00:00AM

---

1 a. RainDance Technologies, Inc.

1 b. 44 Hartwell Avenue

Lexington MA 02421

Sub Contractor Numbers (c):

Patent Clause Number (d-1):

Patent Date (d-2):

Work Description (e): Construction of microfluidic devices

Sub Contract Award Date (f-1): 10/1/2007 12:00:00AM

Sub Contract Est Completion Date(f-2): 8/31/2009 12:00:00AM

Inventions (DD882)

FINAL REPORT

Grant No. W911NF-07-1-0639

A Novel Approach to Chemical Communications (Phase I)

Investigators:

Lawrence S. Bernstein, Spectral Sciences, Inc.
Frank O. Clark, Air Force Research Laboratory, Hanscom AFB
Irving R. Epstein, Brandeis University (PI)
Seth Fraden, Brandeis University
Darren R. Link, RainDance Technologies
Jordan B. Pollack, Brandeis University
Steven Richtsmeier, Spectral Sciences, Inc.
Anatol M. Zhabotinsky, Brandeis University (deceased 9/16/08)

Table of Contents

List of Appendices, Illustrations and Tables

Appendices – Publications

M. Toiya, V.K. Vanag and I.R. Epstein, "Diffusively Coupled Chemical Oscillators in a Microfluidic Assembly," Angew. Chem. Int. Ed. 47, 7753-7755 (2008)

T. Bánsági Jr., M. Leda, M. Toiya, A. M. Zhabotinsky, and I. R. Epstein, "High-frequency oscillations in the Belousov-Zhabotinsky reaction," J. Phys. Chem. A 113, 5644-5648 (2009)

M. Toiya, H.O. Gonzalez-Ochoa, V. K. Vanag, S. Fraden, and I.R. Epstein, "Synchronous Regimes of Oscillatory Microdroplets," J. Phys. Chem. Lett. 1, 1241-1246 (2010).

Illustrations

Tables

I. Introduction

The ultimate goal of this project was to develop a device for encoding and sending modulated high frequency optical signals utilizing a novel combination of chemical oscillators, chemiluminescent reactions and microfluidic technology. Our research team consisted of chemists, physicists and computer scientists from Brandeis University, supported by scientists from Spectral Sciences, Inc. (SSI) and the Air Force Research Laboratory, Hanscom AFB, as well as engineers from RainDance Technologies, Inc. (RDT).

The problem is an extremely challenging one and requires the solution of several subproblems along with integration of those solutions to produce a viable device. Among the tasks that need to be accomplished are: identification and testing of an appropriate chemical reaction or set of reactions capable of producing sufficiently intense chemiluminescence in an appropriate wavelength range and with a useful energy capacity (at least 100 μW/g); design and testing of a microfluidic circuit that makes it possible to generate the desired signal; development of a system that permits the encoding and repeated transmission of messages of 60 characters or more from an alphanumeric character set; construction (or identification) and integration into the circuit of a chemical power source to propel the luminescent material around the circuit; development, analysis and modeling of sensors and algorithms optimized for detection of the signals generated by the device, including construction of a programmable, radiometrically calibrated, modulated light source that is capable of emulating the proposed sources and encoding concepts.

We have made considerable progress toward solving several of these problems and have discovered several potentially significant new phenomena in the course of our investigations. We report these developments below. Nonetheless, there remains significant work to be done in order to produce an operable device. For each aspect of the problem, we outline below the approaches taken and the results obtained, along with brief conclusions about prospects for future success.

II. Research Accomplished

A. Chemiluminescent Reactions

A key element of our approach is the generation of light by a chemiluminescent chemical reaction. We identified and tested several such reactions, both in the near infrared, the wavelength region that we ultimately hope to exploit, and in the visible, which is more convenient for testing the microfluidic circuit and other elements of our device, and which may ultimately prove useful in itself.

1. Singlet oxygen generation

The most promising route to generating continuous high intensity chemiluminescence in the near infrared region (NIR) of the spectrum is through the production of singlet oxygen. The radiative decay of singlet O_2 ($^1\Delta_g \rightarrow {}^3\Sigma_g^-$) results in emission in the NIR at λ = 1270 nm, a wavelength that is ideal for detection. In CCl_4, the quantum yield of this NIR phosphorescence is about 0.07, though this solvent is not ideal because of its toxicity. The thermal decomposition of endoperoxides appears to be the most convenient approach to generating singlet oxygen *in*

situ, and we succeeded in synthesizing 300 mg of 1,4-dimethylnaphthalene endoperoxide (DMNE), the most promising compound we identified.

2. Glowstick Technology

A second approach to producing a continuous source of chemiluminescence is the technology utilized in the production of commercial glowsticks. Visible light of various colors can be generated by the reaction of hydrogen peroxide with a phenyl oxalate ester in the presence of a suitable fluorescent dye. The scheme is shown below.

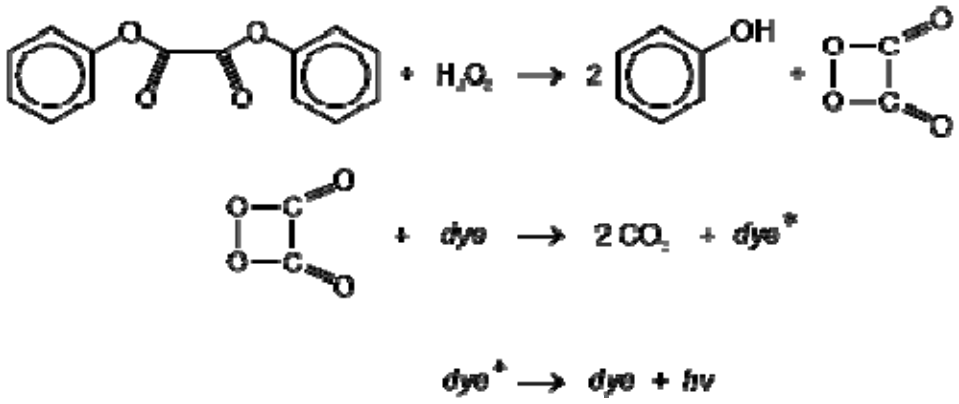

We purchased red glowsticks from a commercial vendor and extracted the reagents to give a convenient and inexpensive source of chemiluminescent material for testing our microfluidic configurations. We also discovered a vendor who manufactures infrared glowsticks for the military (http://glowproducts.com/glowsticks/infraredglowsticks/). We acquired a stock of these and ran some preliminary tests, which suggested that the quantum yield is somewhat less than that of the chemiluminescence produced by DMNE.

3. Luminescent oscillators

An intriguing possibility is to utilize a chemical oscillator as the source of chemiluminescence. We have developed a chemiluminescent oscillator by coupling luminol to the Cu(II)-catalyzed reaction of hydrogen peroxide with potassium thiocyanate in sodium hydroxide (S. Sattar and I. R. Epstein, J. Phys. Chem. 94, 275-277 (1990)). The major limitations on employing this reaction are that it requires a continuous flow of reactants to sustain the oscillation and it oscillates relatively slowly, with a period of many minutes. Recent work in Iran has utilized a variety of organic bases in place of NaOH, resulting in a significant increase in frequency (A. Samadi-Maybodi and R. Akhoondi, Luminescence 23 , 42 (2007)) as well as in intensity and duration of oscillation in a closed system (M.H. Sorouraddin, M. Iranifam and K. Amini, J. Fluor. 18, 443 (2008). We carried out several initial experiments to investigate the feasibility of producing a fast, long-lasting chemiluminescent oscillator, but to date have not succeded in increasing the lifetime enough to make this approach feasible.

4. Hydrogels

A potentially more attractive approach involves coupling the long-lasting BZ oscillator to the luminol reaction in a supramolecular hydrogel. The idea is to utilize the periodic oxidation and reduction of the BZ catalyst to periodically switch the chemiluminescence reaction on and off in order to create a specific pattern of light emission in the hydrogel. Remarkably, the exceptional stability and unique nanofiber matrix of the hydrogel not only give it stability to the extreme conditions (pH 0-1) of the BZ system, but also enhance the intensity of chemiluminescence by improving quantum yield, extend the lifetime of both the catalysts of chemiluminescence and the oscillating reactions by minimizing side reactions, and allow us to control the pattern of emission by tailoring the molecular hydrogelators. We can maximize the compatibility of the chemical oscillating systems with devices by tuning the rheological properties of the hydrogels.

Scheme. Oscillating chemiluminescent supramolecular hydrogels

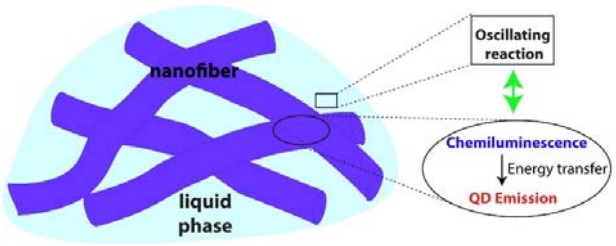

The Scheme at the right outlines the design principle for generating the oscillating chemiluminescent supramolecular hydrogel, a heterogeneous system consisting of a nanofiber matrix and a liquid phase immobilized by the matrix. The substrate and the catalyst for the chemiluminescent reaction can be localized in the nanofiber, while the oscillating reaction occurs in the liquid phase. Because of the nanosize diameter of the fibers and the liquid phase, the substrate, the catalyst, and the components of the oscillating reaction essentially behave as if they were on a surface but able to interact with each other. Such organization mimics the environment of bioluminescence, enabling us to maximize the quantum yield of chemiluminescence and to minimize the decay of the oscillating reaction by confining the BZ reactants to the liquid phase. To tune the wavelength of the emission into the desired range, we can use the chemiluminescence to excite quantum dots incorporated into the nanofibers.

5. Conclusion

If IR luminescence is essential, the DMNE system is probably the best option. Other less toxic aprotic solvents should be investigated to avoid the problems with CCl_4. If an oscillatory signal is desirable, it might be possible to couple this reaction, perhaps in a gel system, to a chemical oscillator. For visible emission, luminol-based reactions offer the advantage of good quantum yield and existing oscillatory behavior. Use of a hydrogel appears to offer the most promising path to increasing the lifetime of the oscillations and the quantum yield of emission.

B. Fast Chemical Oscillation

The Belousov-Zhabotinsky (BZ) reaction, which involves the oxidation by bromate of an organic substrate, typically malonic acid, in the presence of a metal ion or complex as catalyst in a concentrated solution of sulfuric acid, is the best known and most versatile and robust of the oscillating chemical reactions. Unlike most chemical oscillators, which require a continuous flow of fresh reactants to sustain oscillatory behavior for more than a few cycles, the BZ system

will oscillate for several hours and hundreds of cycles in a closed vessel under appropriate conditions. On the other hand, typical BZ oscillations have periods of several minutes or longer, i.e., frequencies of several millihertz. Since we sought to generate signals with frequencies in the range of 10 Hz or more, we decided to try to accelerate the BZ oscillations by three to four orders of magnitude. The key elements in our scheme were to work at higher than normal acid concentrations and temperatures and to vary the concentrations of the reactants and catalyst as well as the identity of the catalyst.

1. Experiments

We carried out an extensive investigation of the parameter space of the reaction, varying temperature, acidity, identity of the catalyst, identity of the substrate, and reactant concentrations. We explored the use of 1,4-cyclohexanedione (CHD) and acetylacetone as alternatives to the usual malonic acid (MA) substrate, but found that malonic acid gives the best performance. Experiments were conducted with cerium (III), manganese (II) and ferroin as catalysts. Temperature was varied from room temperature to over 70 ^{o}C, above which oscillations ceased or became difficult to monitor because of the production of CO_2 bubbles.

Table 1 illustrates typical data with CHD as substrate and ferroin as catalyst. Our best results were obtained with MA and ferroin at a temperature of 60 ^{o}C, where a frequency of 18 Hz was observed.

Table 1. Oscillations in the ferroin-catalyzed BZ-CHD system

Initial Concentrations (M)				T (°C)	F (Hz)
$NaBrO_3$	CHD	Ferroin	H_2SO_4		
0.5	0.6	0.001	1	40	0.5
1	1.2	0.001	1	40	no oscillation
0.5	0.6	0.0005	2	40	1.5
0.4	0.6	0.0005	2	40	1.2
0.3	0.6	0.0005	2	40	1
0.4	0.6	0.0005	3	40	2
0.4	0.6	0.0005	4	40	no oscillation
0.4	0.6	0.0005	2	50	4.5
0.4	0.6	0.0005	2	60	6
0.4	0.6	0.0005	2	65	10
0.4	0.6	0.0005	2	70	13
0.4	0.625	0.0005	2	70	12
0.425	0.6	0.0005	2	70	12
0.5	0.6	0.0005	2	70	no oscillation

Figure 1 shows an example of high frequency oscillations. We were indeed able to increase the frequency of a BZ oscillator by roughly a factor of 5,000, but 20 Hz appears to represent the practical upper limit with this approach, and in a closed system these high frequency oscillations cannot be sustained for more than a few minutes, though with a flow they can presumably continue indefinitely.

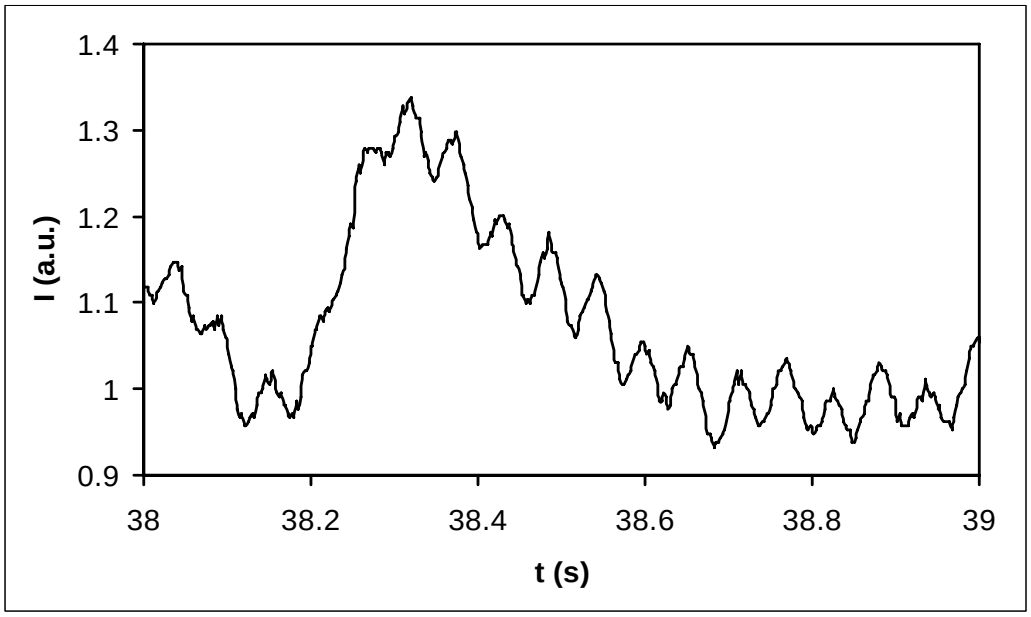

Figure 1. High frequency (18 Hz) oscillations in the ferroin-catalyzed BZ system. Intiital concentrations: $[MA]_0$ = 0.5 M; $[NaBrO_3]_0$ = 0.5 M; $[H_2SO_4]_0$ = 1.14 M; [Ferroin] = 0.0025 M. T = 60 ^oC. Noisy data result from production of CO_2 bubbles, which can be reduced by adding a surfactant.

2. Simulations

We developed a model incorporating all reactant species based on earlier work by Zhabotinsky *et al.* to describe the shape of oscillations and wave properties in the BZ reaction at elevated temperatures. The simplified set of equations used to describe our experimental findings is

$$dX/dt = -k_2h_0XY + k_3h_0AY - 2k_4'X^2 - k_5h_0AX + k_{-5}U^2 + k_6U(C-Z) - k_{-6}XZ \quad (1)$$

$$dY/dt = -k_2h_0XY - k_3h_0AY + qk_7BZ + k_9B \quad (2)$$

$$dZ/dt = k_6U(C-Z) - k_{-6}XZ - k_7BZ \quad (3)$$

$$dU/dt = 2k_5h_0AX - 2k_{-5}U^2 - k_6U(C-Z) + k_{-6}XZ \quad (4)$$

where $X \equiv [HBrO_2]$, $Y \equiv [Br^-]$, $Z \equiv [Ce^{4+}]$, $U \equiv [HBrO_2]$, h_0 is Hammet's acidity function, $A \equiv [NaBrO_3] = h_0/(0.2+h_0)\ [NaBrO_3]_0$, $B \equiv [MA]$, $C \equiv [Ce^{3+}] + [Ce^{4+}]$, and $k_4' = k_4(1+0.87h_0)$. For numerical calculations, based on the initial reactant concentrations, we assigned A_0 = 0.5 M,

B_0 = 2 M, C = 0.001 M, h_0 = 3, which corresponds to $[H_2SO_4]$=1.5 M. The stoichiometric parameter *q* was set to 0.6.

Activation energies calculated by fitting our data were in good agreement with data available in the literature, and the simulations gave good agreement with experiments on the ferroin-catalyzed malonic acid system, as illustrated in Figure 2.

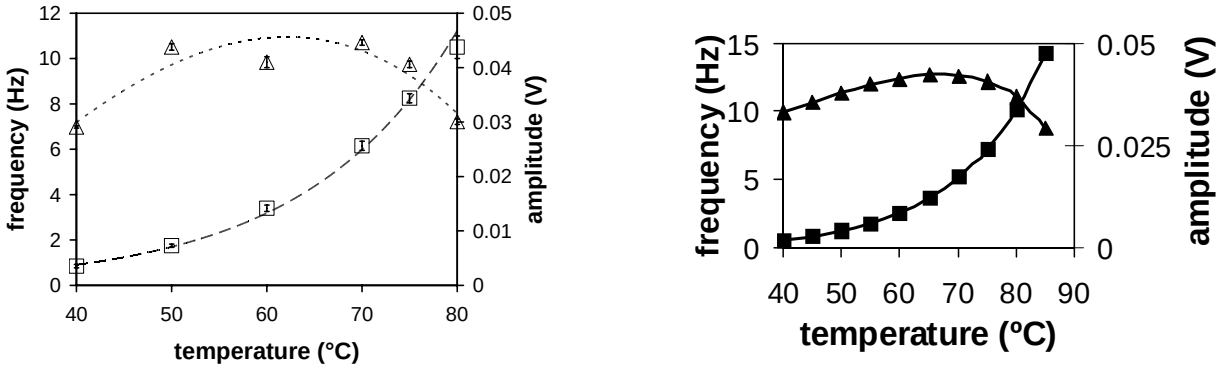

Figure 2. Experimental (left) and simulated (right) frequency (squares) and amplitude (triangles) of oscillation in the BZ system as a function of temperature.

3. Conclusion

We have succeeded in increasing the frequency of oscillation above 10 Hz by manipulating the concentrations and temperature. Under these conditions, the practical upper limit of frequency is about 20 Hz, and the lifetime of the oscillation decreases significantly. The simulations suggest that higher frequencies might be obtainable by putting the system under pressure, which would allow the temperature to be increased beyond 100 ^{o}C. Extending the lifetime would require use of a flow system.

C. Microfluidic Circuitry

A key aspect of our approach was to utilize microfluidic techniques to produce controlled flows of chemiluminescent solutions that will be used to encode the signals. In collaboration with engineers at RDT, we developed and tested several circuits to generate and propel continuous streams of solution or streams consisting of aqueous droplets separated by oil. Since the BZ reactants are polar, the reaction occurs only in the aqueous droplets, though communication is possible between droplets via nonpolar intermediates such as Br_2 that are generated in the reaction and then partition into the oil phase. Since the droplet diameter is comparable to the diffusion length (~ 100 μm), the droplets are internally synchronized by diffusion and require no stirring.

1. One-dimensional experiments

The simplest configuration we explored, and the one that lends itself most easily to the straightforward approach of flowing a stream of drops behind a coded mask, consists of a narrow tube, i.e., a pseudo-one-dimensional (1D) arrangement, which is filled using microfluidic techniques with a fluid composed of aqueous drops containing the luminescent, oscillatory solution separated by an oil phase. The fluid moves at controllable velocities of the order of cm/sec, and drop sizes can easily be varied in the 50-300 μm range. The circuits are constructed from polydimethylsiloxane (PDMS).

Figure 3 shows examples of some tubes containing arrays of BZ droplets. Figure 4 shows the droplets being generated. Table 2 gives a sense of the range of conditions explored and url's for videos of some of the experiments.

.

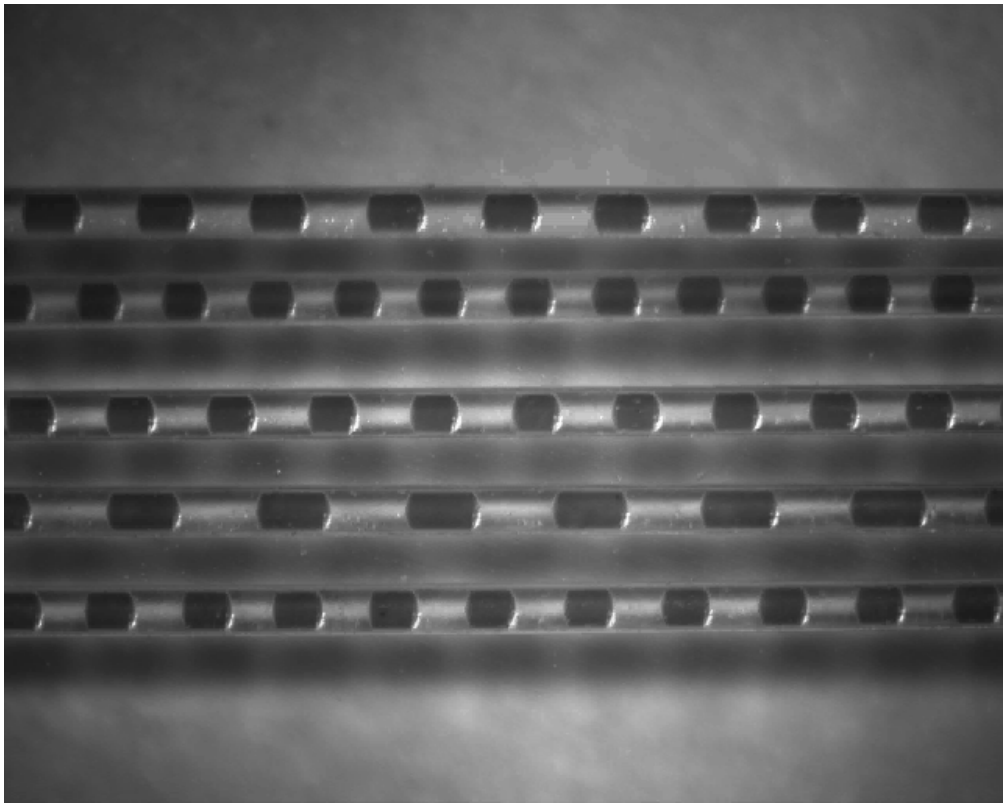

Figure 3. Tubes containing aqueous droplets of varying size and inter-droplet distance with BZ reagent (dark, convex objects) separated by oil (light, concave). Length of tube shown is 4.1 mm; inner diameter of each tube is 150 μm.

Figure 4. Generation of droplets in the microfludic circuit.

Table 2. A sampling of microfluidics experiments

Fluid1 for drop genera-tion	Fluid2 Droplet	Fluid3 for accelera-tion	flow-rate (ul/hr), pressure (psi) fluid1/fluid2/ fluid3	Frequency (Hz) Gen/accel s=stable, a=aperiodic	Speed (mm/s)	Size (microns)	video
Oil (flow)	Water (flow)	Oil (flow)	250/100/500	s1.25/1.25	1.75/4.5	500x335	
			250/100/1000	s1.2/1.2	1.75/6.6	500x335	http://people.brandeis.edu/~ochoa/DARPA/250o1-1hw-1ko2_30fps-150nf.AVI
			250/100/2000	s1.8/1.8	1.75/13	500x335	
			250/100/4000	s1.66/1.66	1.75/44	500x335	
			250/100/7000	a1.76/1.76	1.75/~55	500x335	http://people.brandeis.edu/~ochoa/DARPA/250o1-1hw-7ko2_1kfps-3knf.AVI
			500/300/10000	s2.75/2.75	2.9/43	500x335	
			500/500/20000	s3.75/3.75	-	545x335	
			2000/2000/40000	s14.25/14.25	-	548x335	http://people.brandeis.edu/~ochoa/DARPA/2ko1-2kw-40ko2_1kfps-4knf.AVI
			5000/500/2000	s12.2/12.2	25.6/	293	http://people.brandeis.edu/~ochoa/DARPA/5ko1_5hw_2ko2_1kfps_1knf.AVI
			10000/1000/2000	s25/25		265	
			15000/1500/2000	s45/45		240	
			20000/2000/5000	s60/60		240	
			30000/3000/5000	s99/99		223	http://people.brandeis.edu/~ochoa/DARPA/30k_3k_5k_1kfps_1knf.AVI
Oil (flow)		Air (flow)	200/80/2000	1.3/~1.3 unstable alternating cycle		520x335	http://people.brandeis.edu/~ochoa/DARPA/2ho-8dw-2ka_30fps-1800nf_1.AVI
			200/80/5000	-/~1.4 very irregular			
		Air (pressure)	250/80/2psi	u1.32/aperiodic drop breaking		530x335	
Oil (pressure)	Water (pressure)	-	2.76/1.4	a0.345		470x335	http://people.brandeis.edu/~ochoa/DARPA/pp2.76o1.4wpsi_15fps-1knf.AVI
			3.2/2.3	a0.286		~470x335	
			3.2/2.36	s0.42		~536x335	
			3.5/2.3	a0.58		355x335	
			3.52/1.43	a0.495		357x335	http://people.brandeis.edu/~ochoa/DARPA/pp3.52o1.43wpsi_15fps-1knf.AVI
			5/2.3	a1.18		305	
			5.33/3.85	a*0.588		625x335	
			6.25/2.97	a*1.8		293	
			6.36/3.86	s3.1		424x335	
			6.86/5.64	a*0.416		530x335	http://people.brandeis.edu/~ochoa/DARPA/pp6.86o5.64wpsi_10fps-6hnf.AVI
			7.93/5.64	a*2.4		514x335	

Perhaps surprisingly, the dominant behavior for droplets separated by less than 400 μm is out-of-phase coupling. While intuitively one might expect that bringing the droplets close together would produce in-phase behavior, this turns out not to be the case in the present configuration, at least down to separations of 50 μm. Apparently, the fact that the coupling occurs via bromine, an inhibitor of the reaction, is responsible for this unanticipated behavior. Figure 5 shows some typical results.

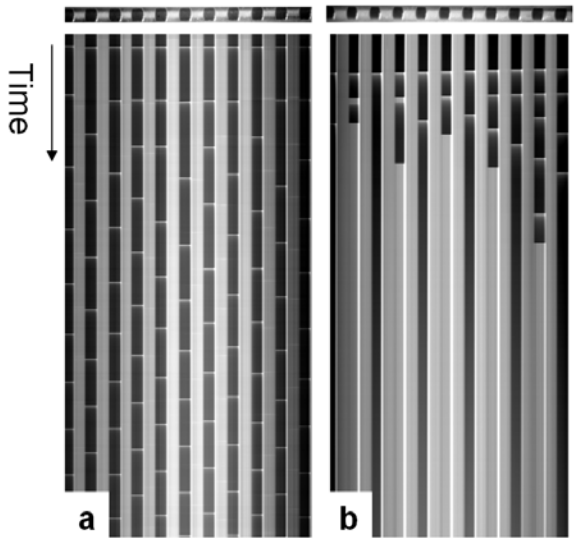

Figure 5. Space-time plots showing (a) anti-phase oscillations with spikes of oxidation of ferroin seen as light horizontal lines across BZ-droplets. (b) stationary Turing structure with alternating oxidized and reduced states evolving from initial oscillatory state. Horizontal length of the frame and the capillary ID are 4.8 mm and 150 μm, respectively; the total times shown in (a) and (b) are 5200 s and 10800 s, respectively. Patterns extend to the left and right of the segments shown.

In the figure, the droplets are the darker vertical columns, separated by the lighter oil columns. The light narrow horizontal stripes are the brief flashes of oxidized ferroin (ferriin) during each cycle. These spikes start off in-phase because the system is initiated with a flash of light to synchronize the drops. In frame (b), where the concentrations are slightly different from frame (a), the oscillations cease after some time, and the system enters a stationary, but patterned, "Turing" state, where alternate drops are either in the oxidized or the reduced state.

2. Two-dimensional experiments

We also used microfluidic techniques to prepare two-dimensional (2D) arrays of BZ droplets in the fluorinated oil HFE-7500. Of course, 2D arrays can give rise to a much richer set of phenomena than 1D arrays, and we have only begun to scratch the surface of what is possible. Earlier experiments at Brandeis on microemulsions consisting of nanometer diameter droplets of a photosensitive aqueous BZ solution in oil showed that this medium can serve as an erasable memory device (A. Kaminaga, V. K. Vanag, and I. R. Epstein, Angew. Chem. Int. Ed. 45, 3087 (2006)). In those experiments, however, the droplets undergo Brownian motion. Here, with the droplets having diameters of roughly 100 μm, the droplets are stationary, and it should be easier to control the patterns. We observed coherent behavior, including regions of in- and out-of-

phase oscillation and traveling waves. Figure 6 shows an example. In other experiments, we observed, after the droplets spontaneously self-assembled into a hexagonal array, a variety of coherent patterns, the most interesting of which consisted of a) a three-phase oscillating pattern, shown schematically in Figure 7, in which all droplets oscillate, with nearest neighbors being 120^o out-of-phase with one another, and b) a two-phase mixed pattern, in which steady state droplets alternate with oscillatory droplets in such a way that neighboring oscillatory droplets are 180^o out-of-phase, and the pattern is symmetric to rotations by 120^o.

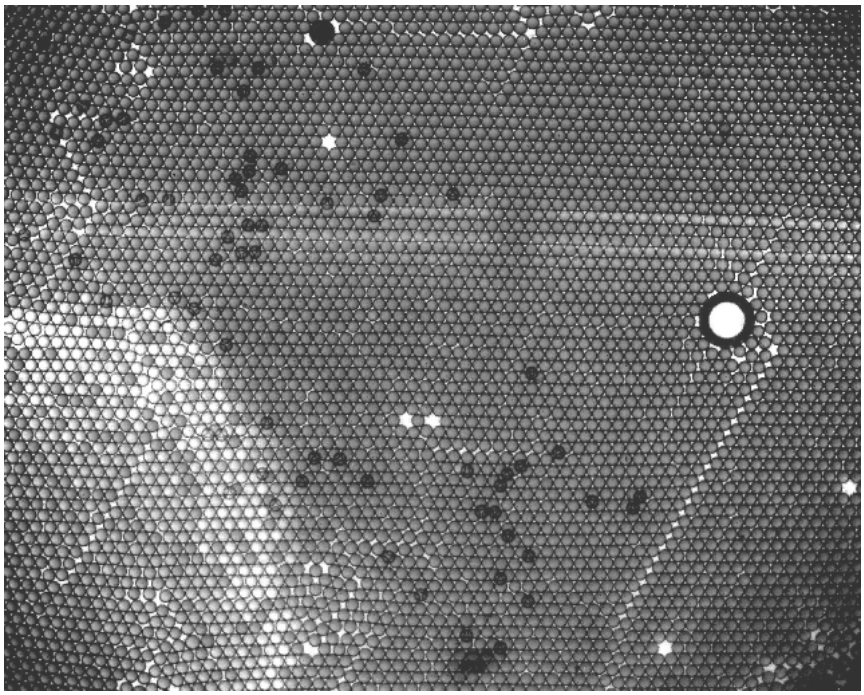

Figure 6. Traveling wave (white area at lower left) of oxidation in a 2D array of BZ water droplets. White "stars" and large white circle are defects and air bubbles.

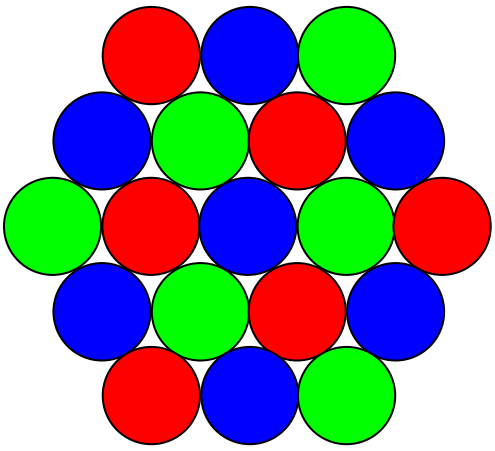

Figure 7. Schematic drawing of the three-phase pattern.

In addition to the emulsion-like arrangement shown in Figure 6, we also explored microfluidic configurations in which droplets can be placed and then connected via narrow channels in any desired 2D arrangement. One such arrangement is shown in Figure 8.

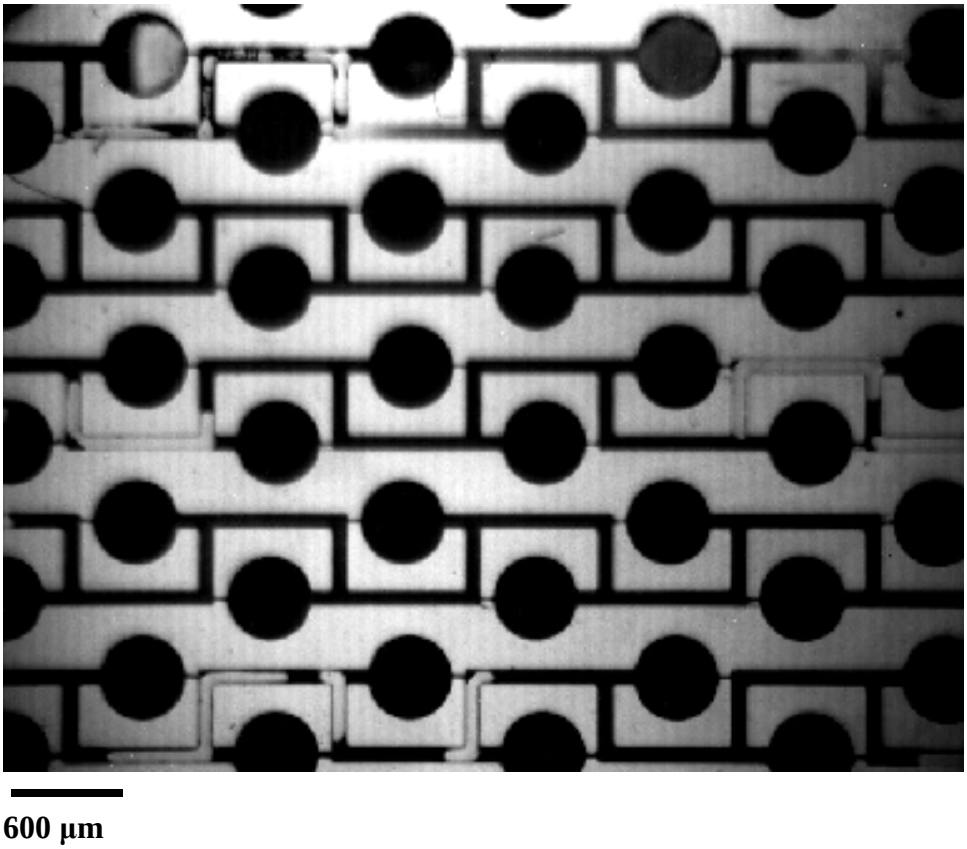

Figure 8. Microfluidic device containing BZ droplets connected by channels.

We also succeeded in creating so-called double emulsions, which offer increased flexibility in linking droplets via either excitatory or inhibitory coupling. A double emulsion ($w_1/o/w_2$) consists of an outer continuous aqueous phase (w_1), a shell of oil (o), and an inner aqueous phase (w_2), which can be different from the outer phase. In our case the two aqueous phases are different BZ solutions and the intermediate oil phase is a fluorinated oil. The process relies on proprietary fluorinated surfactants synthesized by our partner, RDT. Figure 9 shows double emulsions created in preliminary experiments.

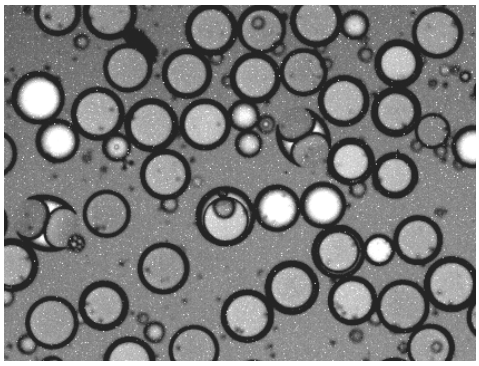

Figure 9. Double emulsion ($w_1/o/w_2$). BZ solution in the oscillatory state is in the core of the drop. BZ solution in the excitable state surrounds the drop. Outer shell of drop is oil

3. Theory

The systems we have explored basically consist of arrays of coupled oscillators, where each BZ droplet constitutes a chemical oscillator, and the coupling arises via nonpolar intermediates produced in the course of the reaction, which travel through the oil phase between adjacent droplets. We have confirmed by addition of a scavenging molecule, as well as by computer simulations, that the species that acts as the "messenger" when the droplets are separated by oil is elemental bromine, a known intermediate of the BZ reaction. Coupled oscillators have the potential to display significantly more complex behavior than individual oscillators. They can generate a variety of phenomena, the simplest of which involve the locking of phases of adjacent oscillators, which can be either in-phase, with all oscillators acting essentially as one, or out-of-phase, typically, but not necessarily, by 180°, so that adjacent oscillators are alternately "on" or "off". If one can understand and control the behavior of such a system of coupled oscillators, it should be possible to exploit the spatiotemporal patterns generated not only for chemical communication but potentially for chemical computation as well.

We have been able to simulate the one- and two-dimensional behavior using a model of the BZ reaction that takes into account the coupling between droplets via bromine. The simulations suggest that more complex patterns can arise. Examples of 1D patterns are shown in Figure 10, and Figure 11 shows 2D patterns. The existence of multiple attracting states suggests that it should be feasible to utilize systems of this type for complex computational as well as communications applications.

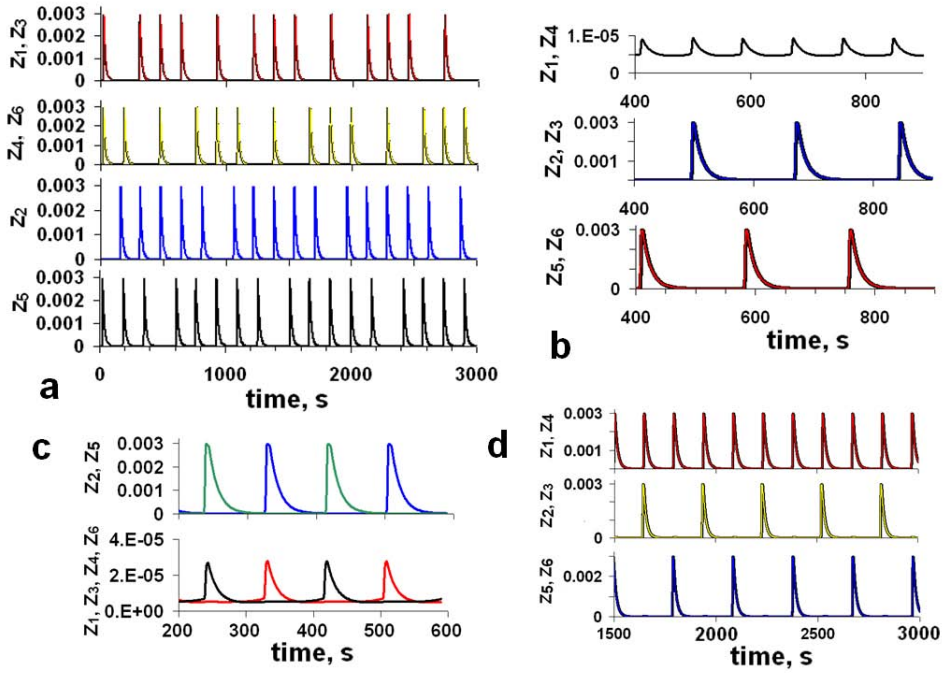

Figure 10. Exotic regimes found in simulations of 6 coupled oscillators at several sets of model parameters. For all simulations initial condition is "almost in-phase," *i.e.*, the phase of one of the six oscillators is slightly shifted. In (a), z_1 and z_3 are in-phase, and z_4 and z_6 also oscillate in-phase. In (b), z_2 and z_3 oscillate in-phase, and z_5 and z_6 are also in-phase, while z_1 and z_4 are almost stationary (small amplitude oscillations). In (c) z_2 and z_5 oscillate out-of-phase, and z_1, z_3, z_4, and z_6 are almost stationary. In (d), z_2, z_3, z_5, and z_6 behave as in (b), but z_1 and z_4 oscillate in-phase with normal amplitude of oscillations and with double frequency. z_i is concentration of variable corresponding to ferroin in the *i'th* oscillator.

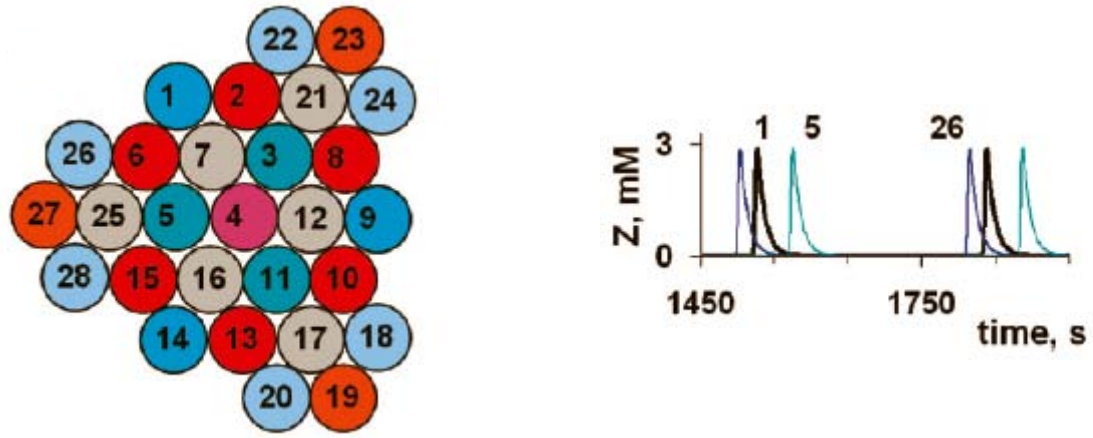

Figure 11. Simulation of a self-assembled hexagonal array of BZ-drops. Left panel shows a 28-drop array, the largest we have simulated to date. The state shown is the "Π-S" state, in which one-third of the drops, shown in gray, are in the oxidized steady state, one-third, shown in blue, oscillate with nearly the same phase, and the other one-third, shown in red, oscillated approximately 180^{o} out of phase with the blue drops. Shades of blue and red indicate relative phases. Differences from perfect antiphase behavior result from differences in numbers of nearest neighbors and distance from the boundary. Right panel shows time series of three blue drops, 1, 5 and 26, illustrating departure from perfect synchrony.

4. Conclusion

This aspect of the project is probably the most promising for future development. The rich behavior of arrays of coupled oscillators offers a wealth of possibilities, both scientific and practical, that we have only begun to explore. While implementation in communications devices remains a challenge, particularly if signals must be transmitted at tens to hundreds of Hz, considerable information density should be attainable. More appealing, though, are applications to "chemical computing," where it should be possible to establish the "rules" that govern how the time evolution of a droplet depends on the states of its neighbors, i.e., one could construct a "chemical cellular automaton." By utilizing the photosensitivity of certain versions of the BZ system, it should be possible to build and control an analog chemically-driven computational device, which would offer advantages for certain types of exponentially difficult (NP-complete) problems, such as routing, scheduling and data retrieval. We have developed both the experimental and the theoretical capabilities to understand these systems in considerable detail.

D. Encoding

We explored two approaches to the problem of encoding the signal generated by the chemical reactions. We report our results below.

1. Crack and Wrap

The scheme we denote as “crack and wrap” involves essentially a single spatial dimension. The reactants are stored in separate compartments, and the reaction is initiated by breaking a barrier that separates them, much as occurs in glowsticks or chemical cold packs. The device is wrapped in a field-printed mask that modulates the visibility of the periodic chemistry into a coded signal from which the message can be recovered. The basic scheme is shown in Figure 12: six channels are used to encode six different frequencies in order to give the six bits required to encode 38 different characters. In the examples shown here, the chemiluminescent solution is a commercial glow stick and the mask is printed on a transparent mylar sheet. The intensity is measured by signal averaging and Fourier transformation of the light from the drops propelled through the circuit. In Figure 13 the intensity of light from one drop is focused on the photomultiplier detector (PMT). The drops generate a square wave signal of light intensity as a function of time as shown in Fig. 13. We generated signals at 65 Hz using syringe pumps to propel the drops. Figure 14 illustrates, with signals from two channels, our ability to extract multiple frequencies, and temporal multiplexing allows us to send sequences of characters. The drops can be transported past the mask either by an external power source or by chemical waves (see below).

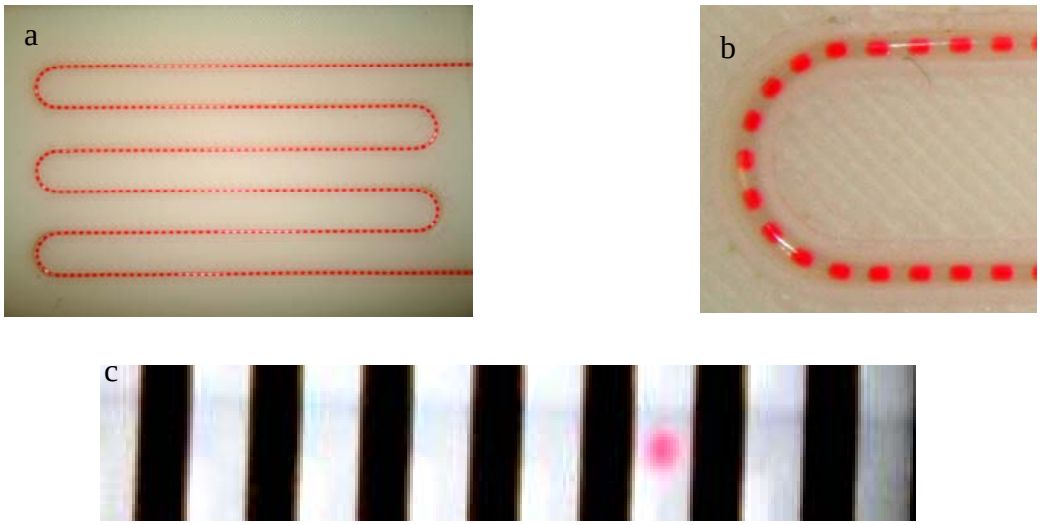

Figure 12. (a) Luminescent drops of 300 μm diameter in cylindrical tubing. (b) magnified view of one bend. (c) a single drop moving under a mask to produce a periodic modulation of the light intensity.

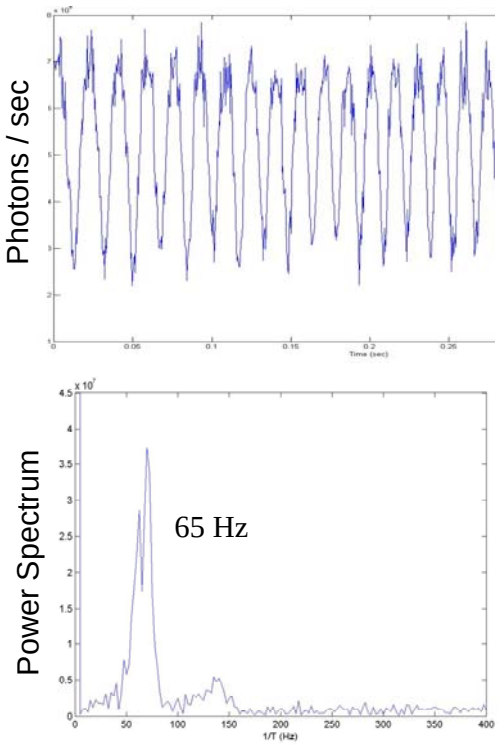

Figure 13. (a) Intensity from luminescent drops of 300 μm diameter moving at 65 Hz through channels. The detector was focused on one drop. (b) Fourier transform of light intensity.

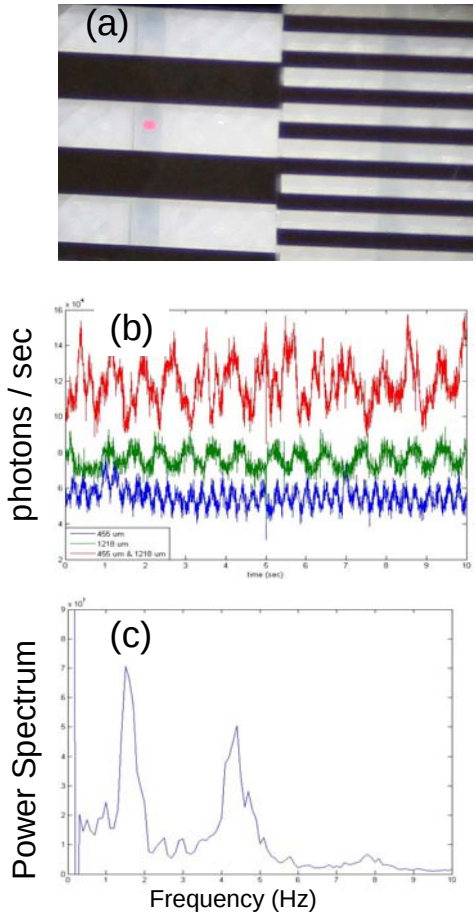

Figure 14. (a) Different masks over each of the six lines shown in Fig 4. (b) Intensity vs. time of drops moving under one mask at a time (green, blue) and under two masks simultaneously (red). (c) FFT of red trace in (b). The FFT shows two frequencies, corresponding to drops simultaneously moving under two masks.

2. Spray and Display

The second scheme, "spray and display," utilizes two spatial dimensions. Here the reactants of the photosensitive $Ru(bpy)_3$-catalyzed BZ reaction and the supporting emulsion are mixed in an aerosol can containing multiple chambers and microfluidic circuitry and propelled onto a prepared surface, where they self-assemble into a regular lattice, e.g., hexagonal. The technology is similar to that needed to produce the foam that comes out of a shaving cream can. Alternatively, the target surface can be pre-patterned with a desired array of drop locations and connections as in Fig. 8. With the photosensitive reaction, the initial condition can be set by projecting the desired pattern onto the lattice. This "chemical cellular automaton" will then evolve, producing a long-lasting repetitive pattern that corresponds to the message. The set of initial conditions and patterns associated with the array of possible messages can be developed through extensive simulations and experimentation and stored in a codebook.

3. Conclusion

The "crack and wrap" approach appears feasible for a 1D system. Considerable additional work needs to be done to establish the feasibiity of the "spray and display" approach.

E. Power Source

In order for approaches involving luminescent materials flowing behind masks to be successful, it is necessary to have a means of creating a flow of fluid through the system. We have explored several approaches to this problem.

1. Gas Pressure

Our initial proposal was to propel material through the microfluidic system by generating a gas that would create sufficient pressure, i.e., to construct a device analogous either to an air bag or a pressure cooker. On further consideration, we concluded that such approaches are likely to be subject to a variety of technical problems involving the ability to control the gas pressure.

2. Chemical Waves

A much simpler approach is to initiate a chemical wave that would carry the information, obviating the necessity for a bulk flow of material. We have been able to generate waves not only in continuous media, but also, as illustrated in Fig. 6, in one- and two-dimensional arrays of droplets. Whether this approach is compatible with the desired information density remains to be established.

3. Other Approaches

In our experiments, we used syringe pumps to drive fluid through the system. This approach is clearly not adaptable to the size of device that we ultimately sought to build. Two other approaches do seem possible. A relatively simple solution is to employ printable zinc-air microbatteries (http://ccsl.mae.cornell.edu/research/sff/index.htm), which can provide sufficient

power at very little cost in terms of added mass or space occupied. It may also be possible to incorporate magnetic nanoparticles into the fluid and then use a spinning magnet driven by a tiny motor to generate the force to move the fluid.

4. Conclusion

This area is the one in which we have made the least progress. If our approaches were to be carried further, considerably more work would need to be devoted to power sources. The most promising approach appears to be the use of small batteries, perhaps of the zinc-air type noted above.

F. Signal Detection

The SSI and AFRL members of the team focused their efforts on the issue of how the signals generated by the device can be detected in an environment that contains a high level of temporally varying optical noise. To deal with this issue, they a) developed a programmable simulator to mimic the signals to be generated by the chemical communications device; and b) carried out field tests to assess how bright a modulated source might have to be to enable us to distinguish it from temporal components of naturally varying backgrounds. We discuss progress in each of these areas below.

1. Programmable simulator

The basic design of the simulator is shown in Figure 15. It consists of an array of six infrared LEDs. Each LED is individually controllable for brightness and modulation, and there is one controller channel per LED and one analog voltage output from the PC for each controller channel. Band pass filters (BP) are used to select wavelengths not at the LED peak. Neutral density filters (ND) provide an additional level of power control, and the diffuser (DF) is available to modify the directional LED output.

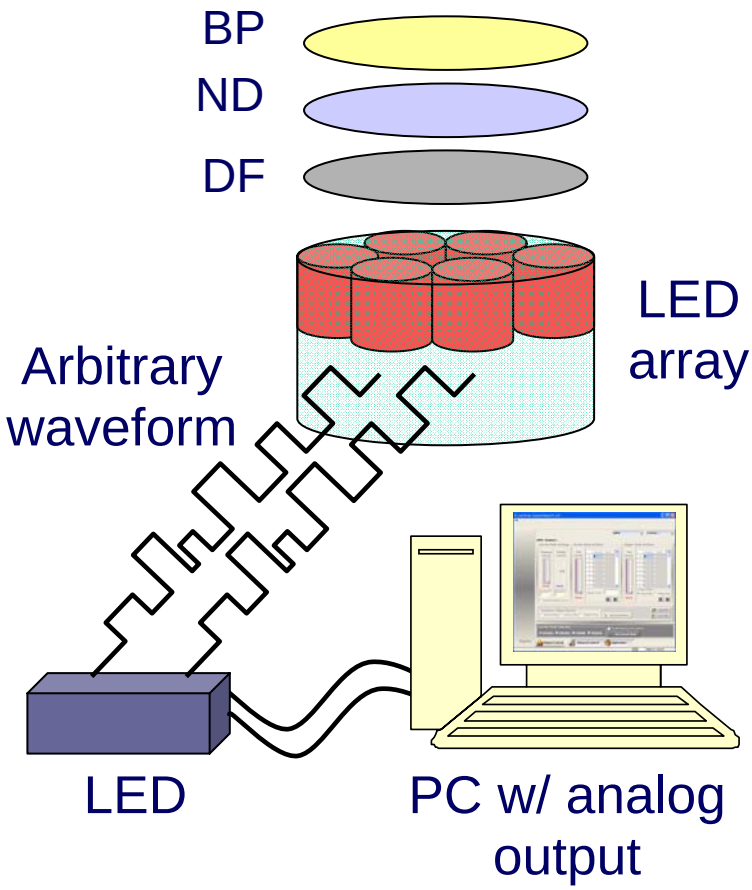

Figure 15. Basic layout of the programmable source simulator.

2. Field Measurements

On June 10, 2008, we took advantage of an opportunity to utilize AFRL instrumentation to monitor a modulated light source in a natural setting. The purpose of the measurements was to develop an understanding of how bright a modulated source might have to be to be able to distinguish it from temporal components of naturally varying backgrounds.

A suite of instrumentation was located in the Yankee Building atop Mt. Washington, including radiometers with a cutoff filter at 0.85, and band pass filters at 1.25±0.075 and 1.6 ±0.1 μm, respectively. In addition, an infrared imager (Sensors Unlimited, Inc. SU640) fitted with a 1.6 μm filter was utilized. The radiometer signals were sampled at 20 kHz. The SU640 imager was operated at a 120 HZ frame rate in 256 x 256 pixel mode. The radiometer fields-of-view were all 9.7°, and the imager FOV was 49.1°. Figure 16 shows the view from the Yankee Building atop Mt. Washington looking westward toward the parking lot of the Cog Railway Station, where the light source was operated. The range from the instrument suite to the parking lot was 4.16 km

Figure 16. Clear LOS view from inside the Yankee Building atop Mt. Washington, looking westward toward the parking lot of the Cog Railway Station (the beige pixels at the center of the red circle).

The light source was a 100 W halogen spot light with a 9° beam width, equipped with a Variac voltage control. When operated at full power, the bulb is about 80% efficient with a spectral output that looks like a 3000 K black body. Total in-band, in-beam power is about 7-8 W in each of the 1.2 and 1.6 μm spectral band passes. The source was mounted behind a 20" five-blade three-speed box fan equipped with a variable voltage control to adjust the speed. The maximum modulation rate for this setup was 80 Hz.

a. Sample results

Figure 17 shows the raw radiometer signal for the 1.2 μm band pass. For this particular experiment, the light source was chopped at 72 Hz and turned on full power at t~10 sec, then the source intensity was gradually decreased over the course of tens of seconds, then turned on back to full power at t~170 sec. There is no clear indication of any of these events in Figure 17. Over the course of this run, there were scattered clouds above summit altitude passing through the scene. All of the temporal variations in the figure are due to time varying shadows in the radiometer FOV. Since the radiometer FOV is quite wide (9.7°) and the clouds were at about summit level, cloud movement can cause gross changes in the total signal observed in the space of seconds. Similar behavior was observed in the 1.6 μm channel (Figure 18).

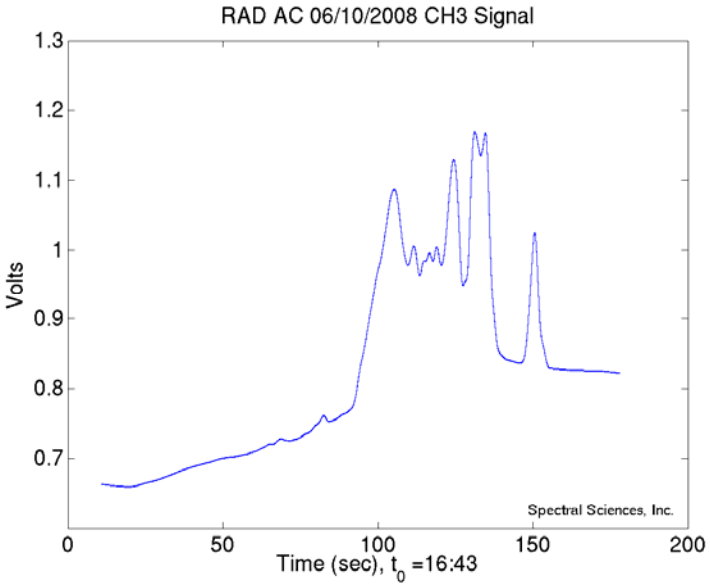

Figure 17. Raw radiometer signal for the 1.2 μm band pass.

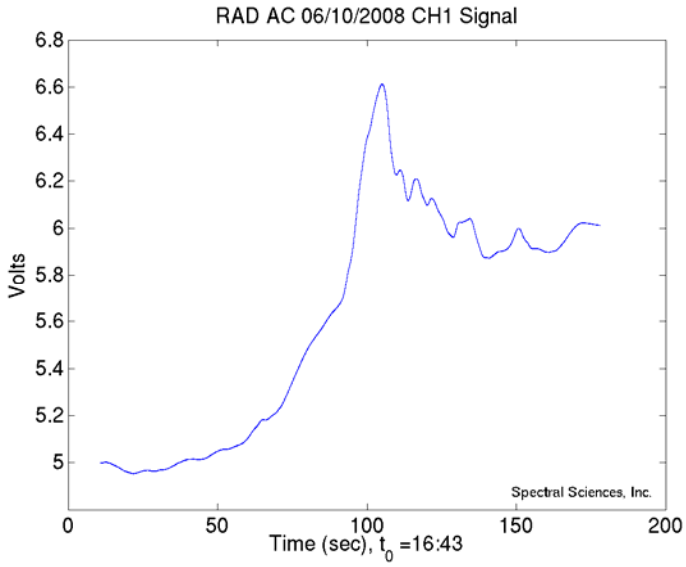

Figure 18. Raw radiometer signal for the 1.6 μm band pass.

In order to pull out the modulated source contribution to the full raw radiometer signal, we typically process the data in the following way. First the data is de-trended by subtracting off the running average from a one second smoothing window, effectively removing the DC component as well as frequencies below 1 Hz from the power spectrum. Then a Fourier transform is performed on the data in 1 sec chunks. The result is a power spectrum as a function of time with low frequencies removed. Figure 19 shows the result using the radiometer data of Figure 17. In this display, fixed frequency events show up as vertical lines. In Figure 19, there is a vertical line at 72 Hz that shows up at the top of the figure and decreases in intensity with time until it is indistinguishable from the background, then appears again at 170 s when the source is returned to full power. Figure 20 shows similar behavior for the 1.6 μm channel. The difference here is that there appears to be much less background interference at lower frequencies at 1.6 μm than for 1.2 μm, with the result that the source at 72 Hz is easier to pick out. (The prominent feature at 60 Hz is due to pickup of line voltage at some point in the instrument detection stream.)

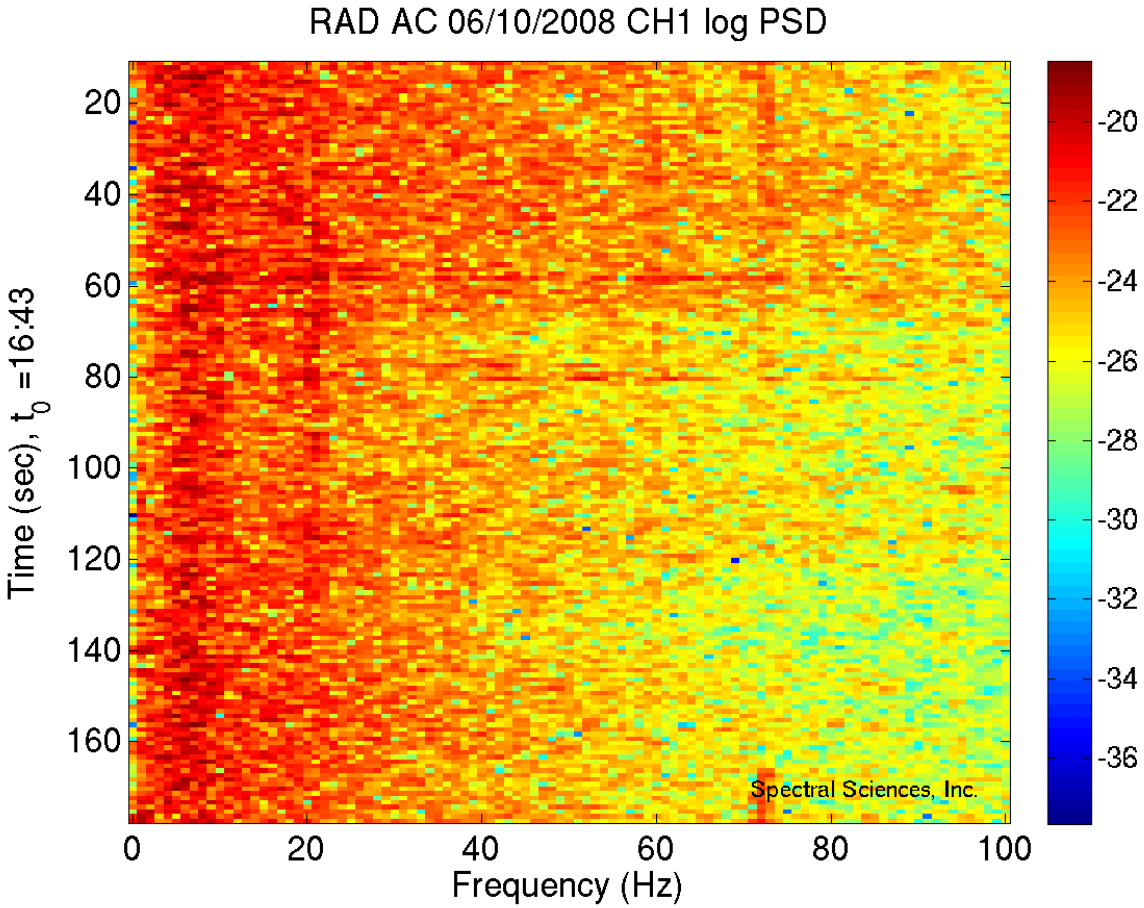

Figure 19. Log of the power spectral density as a function of time for the 1.2 μm radiometer channel.

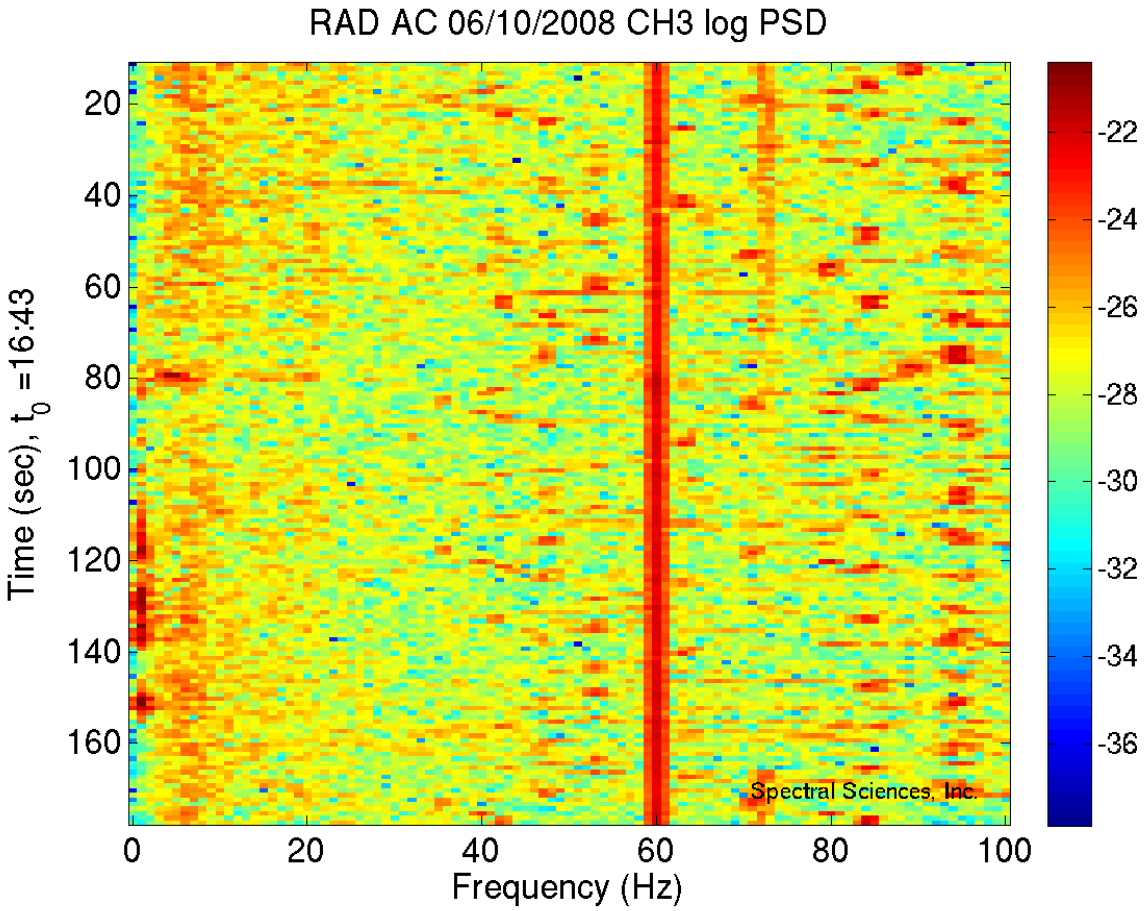

Figure 20. Log of the power spectral density as a function of time for the 1.6 μm radiometer channel.

Figure 21 shows a sample frame of processed data from the SU640 imager. Processing of this data was performed as for the radiometers, except that it was performed pixel by pixel for each pixel in the display. We also include a spatial averaging over ~3 pixels to suppress temporal changes caused by pixel to pixel movement of scene features. The results are presented as a quad with the display at the upper left being raw imager data, and the display at the upper right being an RMS image. At the lower left is pixel power summed over a range of frequencies, in this case, wide enough to select the frequency of the modulated light source. Finally, at the lower right is a combination of vectors resulting from principal component analysis of the data. Though there is no indication of the light source in the raw image, it is clearly apparent as the bright yellow spot just over the rock ledge in the RMS image. The source is also visible in the corresponding position of the frequency slice at the lower left, though it is not so obvious, as there are several interferences, such as a patch of sunlight traveling over the rock ledge in the near field at the same time. The PCA image at the lower right shows little or no evidence of the source.

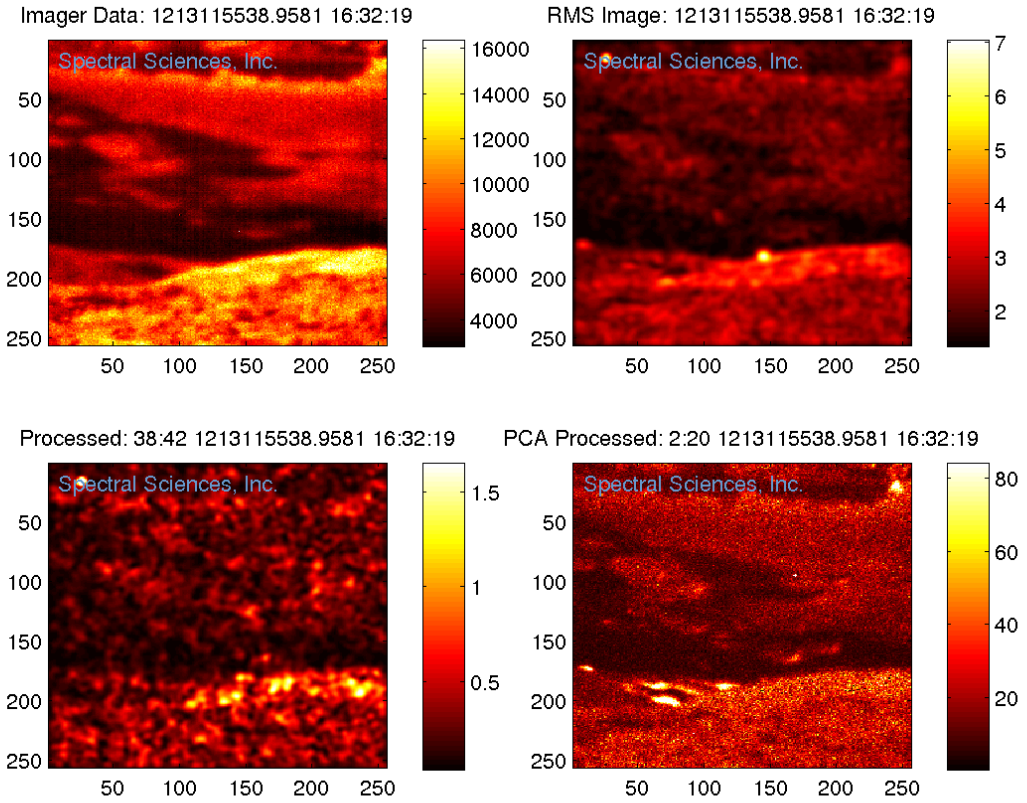

Figure 21. Quad display of processed output from the SU640 infrared imager (see text).

3. Conclusion

The simulator provides a valuable tool for testing detection capabilities, and the ability of the SSI team to carry out field tests and analyze signals generated should prove valuable in assessing the capabilities of whatever method is eventually chosen to implement the desired goals for chemical communication.

III. Publications

This work has resulted in three publications:

M. Toiya, V.K. Vanag and I.R. Epstein, "Diffusively Coupled Chemical Oscillators in a Microfluidic Assembly," Angew. Chem. Int. Ed. 47, 7753-7755 (2008)

T. Bánsági Jr., M. Leda, M. Toiya, A. M. Zhabotinsky, and I. R. Epstein, "High-frequency oscillations in the Belousov-Zhabotinsky reaction," J. Phys. Chem. A 113, 5644-5648 (2009)

M. Toiya, H.O. Gonzalez-Ochoa, V. K. Vanag, S. Fraden, and I.R. Epstein, "Synchronous Regimes of Oscillatory Microdroplets," J. Phys. Chem. Lett. 1, 1241-1246 (2010).

Copies of these works appear in the Appendix below.

Angewandte Chemie

Synchronized Nano-Oscillators

DOI: 10.1002/anie.200802339

Diffusively Coupled Chemical Oscillators in a Microfluidic Assembly**

*Masahiro Toiya, Vladimir K. Vanag, and Irving R. Epstein**

From fireflies that synchronize their flashes with each other[1] to heart muscles contracting and relaxing in unison,[2] synchronized behavior of living cells or organisms is ubiquitous in nature.[3] Chemical reaction–diffusion systems can help us understand the mechanisms that underlie such synchronization. Coupled chemical oscillators have previously been studied in the laboratory with large reactors connected directly by small channels for controlled mass exchange of bulk solution.[4–7] In this case, coupling occurs via all species. In living systems, however, coupling often occurs through special signaling molecules, as in synaptic communication or chemotaxis.[8] Collections of neural oscillators can access a vast repertoire of coordinated behavior by utilizing a variety of topologies and modes of coupling, including gap junctions and synaptic links, which may be either excitatory or inhibitory, depending on the neurotransmitter involved.

To mimic such a fine level of communication in a chemical system, we need to do two things: a) reduce the size of each oscillator in order to bring the characteristic time of communication between diffusively coupled oscillators to or below the period of oscillation; and b) introduce a semipermeable membrane or other medium between the microoscillators to permit communication only via selected species. These goals can be achieved with the use of microfluidic devices. Our experimental system (Figure 1 a) is a linear array of tens of droplets of nanoliter volume containing aqueous ferroin-catalyzed Belousov–Zhabotinsky (BZ)[9] solution separated by octane drops in a glass capillary. The BZ reaction, in which the oxidation of malonic acid (MA) by bromate is catalyzed by a metal complex in acidic aqueous solution, is a well known chemical oscillator. Owing to the small spatial extent ($l_w = 100$–400 μm) of the BZ droplets, the characteristic time of diffusive mixing within a single droplet, l_w^2/D (5–80 s, D = diffusion constant of aqueous species), is smaller than the period of oscillation (180–300 s), and individual BZ droplets can be considered homogeneous. Bromine, an inhibitory intermediate of the BZ reaction, is quite hydrophobic and diffuses readily into hydrocarbons such as octane, thus mediating inhibitory interdroplet coupling. We have shown

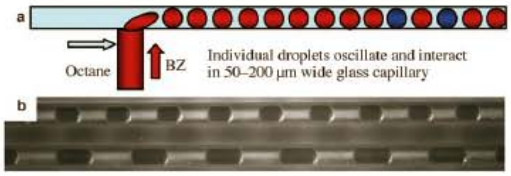

Figure 1. a) Schematic representation of the microfluidic device. Red droplets correspond to the reduced form of the catalyst (ferroin), blue droplets to the oxidized form (ferriin). A new method for fabricating such junctions is outlined in the Supporting Information. b) Snapshot of two capillaries with droplets. BZ droplets with convex surfaces are dark due to ferroin. Horizontal length of the frame and inner diameter (ID) of the capillary are 4.8 mm and 150 μm, respectively. BZ droplets were recorded by a CCD camera through a microscope with illumination by light passed through a 510 nm interference filter.

theoretically[10] that in such heterogeneous systems patterns analogous to the Turing patterns[11,12] found in homogeneous systems can emerge.

Without compartmentalization, the homogeneous BZ solution in a similar capillary exhibits trigger waves of excitation. Partitioning the medium into droplets dramatically changes this behavior. For BZ droplets (Figure 1 b) with $l_w > 400$ μm or oil droplets with length $l_O > 400$ μm, no discernible coherent patterns are seen. However if $l_w = 100$–400 μm and $l_O = 50$–400 μm, we observe stable anti-phase oscillations (Figure 2 a) at larger [MA] (greater than 100 mM) and Turing patterns (Figure 2 b) at smaller [MA] (less than 40 mM). At higher levels of [MA], initially in-phase arrays of droplets evolve to an anti-phase configuration within a few periods of oscillation (Movie in Supporting Information). For [MA] = 40 mM, the transition to the Turing regime goes through intermediate anti-phase oscillations. For slightly smaller [MA] (35 mM), initially in-phase droplets transform into Turing patterns almost immediately, without intermediate anti-phase oscillations. At small [MA], the behavior is rather sensitive to the size of droplets, with small drops reaching stationary state more rapidly than larger ones.

To establish whether bromine is responsible for communication between the BZ droplets, surfactant Span 80 (sorbitan mono-oleate) at concentrations of 5 % was added to the octane. In separate experiments, it was found that Span 80, which possesses an unsaturated double bond in its hydrocarbon tail, reacts with bromine in octane in less than 1 s. The water-insoluble Span 80 thus acts as a trap for bromine, removing it from the octane. When Span 80 is added to the droplet system, inhibiting the communication between BZ droplets, individual droplets oscillate independently. If we initiate the system (see Experimental Section) with all droplets in the same phase, in-phase oscillations persist.

[*] Dr. M. Toiya, Prof. V. K. Vanag, Prof. I. R. Epstein
Department of Chemistry and Volen Center for Complex Systems
MS015, Brandeis University, 415 South St., Waltham, MA 02454 (USA)
Fax: (+1) 781-736-2516
E-mail: epstein@brandeis.edu
Homepage: http://hopf.chem.brandeis.edu/

[**] This work was supported by the National Science Foundation (CHE-0615507) and the Defense Advanced Research Projects Agency. We thank Milos Dolnik and Anatol Zhabotinsky for helpful comments and suggestions.

Supporting information for this article is available on the WWW under http://dx.doi.org/10.1002/anie.200802339.

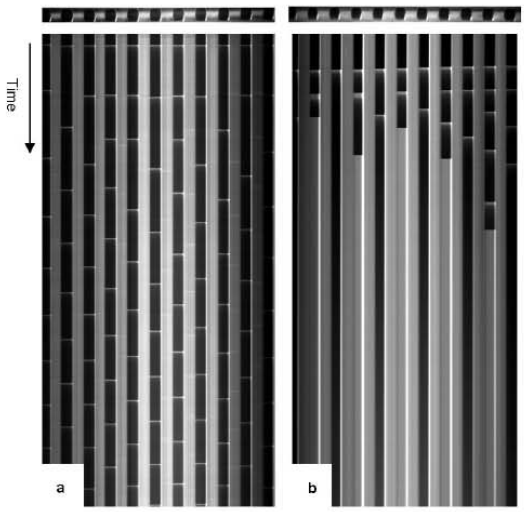

Figure 2. Space–time plots showing a) anti-phase oscillations with spikes of oxidation of ferroin seen as light horizontal lines across BZ-droplets and b) stationary Turing structures with alternating oxidized and reduced states evolving from an initial oscillatory state. Horizontal lengths of the frame and the capillary ID are 4.8 mm and 150 μm, respectively; the total times for (a) and (b) are 5200 s and 10800 s, respectively. Patterns extend to the left and right of the segments shown.

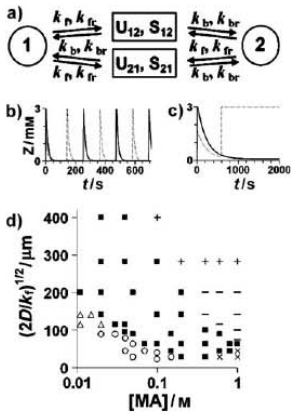

Figure 3. a) Configuration of two coupled BZ oscillators used in simulations. b) Typical anti-phase oscillations. c) Typical Turing mode; bold and dashed lines in (b) and (c) represent z in two neighboring BZ droplets. d) Parametric diagram in [MA]–k_f plane for two oscillators whose initial phases are slightly shifted ($k_b = k_f/P_U$, $k_{br} = k_{fr}/P_S$; partition coefficients $P_U = 20$, $P_S = 1$, $[H^+] \equiv h = 0.2$ M, $[BrO_3^-] \equiv A = 0.3$ M, $z + c = 3$ mM); $D = 2 \times 10^{-5}$ cm^2 s^{-1} is used for conversion of k_f into a characteristic length $L = (2D/k_f)^{1/2}$. Symbols: ○ and △: Turing mode for $k_{fr} = 0$ and for both $k_{fr} = 0$ and $k_{fr} = k_f$, respectively; ■: anti-phase oscillations; −: unstable in-phase oscillations transforming into anti-phase oscillations for larger number (four or six) of coupled oscillators; ×: stable in-phase oscillations (for $k_{fr} = 0$); Turing mode marked by ○ is replaced by in-phase oscillations (×) for $k_{fr} = k_f$; +: weak communication (initial phases of oscillators change very slightly after ten periods of oscillations). Subscripts "12" and "21" refer to U ($[Br_2]$) and S ($[BrO_2^{\bullet}]$) in octane droplets.

Seeking to understand our experimental results in more depth, we performed a series of computer simulations to ascertain whether bromine is the single, or at least the major, signaling molecule, and whether other patterns may be found at smaller droplet sizes inaccessible in our experiments. The BZ reaction generates a second, excitatory intermediate, $BrO_2^{\bullet}$, which is also capable of diffusing in the oil phase. The model, which is described in detail in the Supporting Information, is based on the Field–Körös–Noyes (FKN) mechanism[13] of the BZ reaction and employs seven concentration variables to describe the aqueous phase and two more, corresponding to $[Br_2]$ and $[BrO_2^{\bullet}]$, for the oil phase. The concentrations of the major reactants, H^+, MA, BrMA, and BrO_3^- which are significantly larger than those of the variable species, are taken to be fixed in a given experiment. The model contains $9n$ variables for n coupled oscillators. In addition to the initial concentrations, key parameters in the model include the coupling constants, k_f and k_{fr}, which characterize the strength of coupling mediated by Br_2 and $BrO_2^{\bullet}$, respectively. We simulated arrays with two (Figure 3a), four, and six coupled oscillators to investigate how the behavior of the system depends on the number of oscillators.

The two stable modes found in the experiments, anti-phase oscillations and Turing patterns, are seen in the model at large and small [MA], respectively, and are shown in Figure 3b and c. Note that if $k_f = 0$, that is, coupling via Br_2 is absent, neither the anti-phase oscillations nor the Turing mode occurs, so Br_2 is an essential "messenger" for these two regimes. At higher [MA] (greater than 0.2 M), where the anti-phase mode dominates, the results of the simulation are nearly independent of the presence of $BrO_2^{\bullet}$, while at lower [MA] (less than 0.1 M) and at large k_f (greater than 0.5 s^{-1}), the Turing mode dominates at $k_{fr} = 0$ and the in-phase mode dominates at $k_{fr} = k_f$ (Figure 3d). Since at $k_{fr} = k_f$ the Turing mode is found only at [MA] < 20 mM, while in our experiments we found the Turing mode at larger [MA] (40 mM), we infer that $BrO_2^{\bullet}$ plays a minor, if any, role in communication between the BZ droplets.

For many sets of parameter values, two or more modes are simultaneously stable, and the mode obtained depends upon the initial conditions. Simulations with four and six oscillators, however, reveal that, when they coexist, the in-phase mode is always less stable than the Turing or anti-phase modes. Stable in-phase behavior is found only at large $k_{fr} = k_f$, corresponding to very small droplet lengths (less than 100 μm). With such small droplets, we also find several more exotic regimes, some of which are illustrated in the Supporting Information.

Chemical nano-oscillators diffusively coupled by known signaling species may provide useful analogs for biological processes. The microfluidic BZ–octane system employed here is convenient in that we are able to identify the inhibitor bromine as the main messenger species, and the production and function of bromine in the overall BZ process are well characterized. By choosing the fundamental oscillator and the scavenger species added to the connecting medium, it should be possible to build systems with controllable degrees of

inhibitory or excitatory coupling. Microfluidic technology makes it possible to construct two- as well as three-dimensional arrays of coupled oscillators. The possibility of developing computational devices by combining oscillatory chemical reactions with droplet-based microfluidic techniques has recently been suggested.[14]

Experimental Section

BZ mixture: The aqueous reaction mixture contains H_2SO_4 (80 mM), $NaBrO_3$ (0.288 M), and ferroin (3 mM). In addition, for experiments on the oscillatory mode we add NaBr (10 mM) and MA (0.64 M), while for experiments on Turing patterns [NaBr] = 0, [MA] = 30–50 mM. To make the BZ reaction photosensitive, we add a small amount (0.4 mM) of [Ru(bpy)$_3$] (bpy = bipyridine).[15]

Microfluidics: The BZ solution and octane are driven by syringe pumps into a microfluidic junction at the entrance to the capillary as shown in Figure 1 a. The sizes of and separation between the BZ droplets depend upon the junction size and the flow rates with which the two components are injected into the system.[16] Before the start of each experiment, we put the BZ micro-oscillators into the in-phase mode by illuminating the capillary with a strong 450 nm light. Further technical details are given in the Supporting Information.

Received: May 19, 2008
Published online: August 29, 2008

Keywords: Belousov–Zhabotinsky reaction · coupled oscillators · microfluidics · oscillatory reactions · synchronization

[1] A. Moiseff, J. Copeland, *J. Insect Behav.* **2000**, *13*, 597.
[2] L. Glass, *Nature* **2001**, *410*, 277.
[3] A. Pikovsky, M. Rosenblum, J. Kurths, *Synchronization: A Universal Concept in Nonlinear Science*, Cambridge University Press, Cambridge, **2001**.
[4] M. Marek, I. Stuchl, *Biophys. Chem.* **1975**, *3*, 241.
[5] M. Dolnik, M. Marek, *J. Phys. Chem.* **1988**, *92*, 2452.
[6] G. Dechert, K. P. Zeyer, D. Lebender, F. W. Schneider, *J. Phys. Chem.* **1996**, *100*, 19043.
[7] M. F. Crowley, I. R. Epstein, *J. Phys. Chem.* **1989**, *93*, 2496.
[8] H. C. Berg, *E. Coli in Motion*, Springer, New York, **2004**.
[9] A. M. Zhabotinsky, *Proc. Acad. Sci. USSR Chem. Sect.* **1964**, *157*, 4.
[10] V. K. Vanag, I. R. Epstein, *J. Chem. Phys.* **2003**, *119*, 7297.
[11] A. M. Turing, *Philos. Trans. R. Soc. London Ser. B* **1952**, *237*, 37.
[12] V. Castets, E. Dulos, J. Boissonade, P. De Kepper, *Phys. Rev. Lett.* **1990**, *64*, 2953.
[13] R. J. Field, R. M. Noyes, E. Körös, *J. Am. Chem. Soc.* **1972**, *94*, 8649.
[14] I. R. Epstein, *Science* **2007**, *315*, 775.
[15] V. Gáspár, G. Bazsa, M. T. Beck, *Z. Phys. Chem.* **1983**, *264*, 43.
[16] T. Ward, M. Faivre, M. Abkarian, H. A. Stone, *Electrophoresis* **2005**, *26*, 3716.

High-Frequency Oscillations in the Belousov−Zhabotinsky Reaction

Tamás Bánsági, Jr., Marcin Leda, Masahiro Toiya, Anatol M. Zhabotinsky,† and Irving R. Epstein*

Department of Chemistry and Volen Center for Complex Systems, MS 015, Brandeis University, Waltham, Massachusetts 02454-9110

Received: February 12, 2009; Revised Manuscript Received: March 17, 2009

Chemical oscillations in the classic Belousov−Zhabotinsky (BZ) system typically have a period of a few minutes, which can be increased significantly by changing the organic substrate. Here we show that by changing the temperature and concentrations, an increase of 3−4 orders of magnitude in the *frequency* of BZ oscillations can be obtained. At elevated temperatures, in high concentration mixtures, the cerium-catalyzed reaction exhibits sinusoidal oscillations with frequencies of 10 Hz or greater. We report the effect of temperature on the frequency and shape of oscillations in experiments under batch conditions and in a four-variable model. We show that our simple model accurately captures the complex temporal behavior of the system and suggests paths toward even higher frequencies.

Introduction

The Belousov−Zhabotinsky (BZ) reaction[1,2] continues to draw considerable scientific interest even five decades after its discovery. Over the years, the name has come to refer to a family of metal-ion-catalyzed, bromate-driven reactions in which organic substrates in acidic media are oxidized to give oscillations in the concentrations of various intermediates. The detailed mechanism of the classical, cerium-ion-catalyzed reaction system was first described by Field, Körös, and Noyes[3] (FKN). By reducing its complexity to a few coupled elementary pseudoreactions, Field and Noyes were able to construct a simplified mathematical model,[4] now known as the Oregonator, which exhibits oscillatory limit cycles. The model also successfully describes a wealth of complex phenomena seen in the BZ reaction, both temporal, such as excitability,[5,6] bistability,[7] stirring effects,[8,9] quasiperiodicity, and chaos,[10,11] and spatial, including traveling waves,[12] target and spiral patterns,[13,14] scroll rings,[15] and their orientation dynamics in advective fields.[16]

The Oregonator has been also used to model the effect of temperature on oscillations, prompted by Körös' experimental study[17] of the BZ reaction between 15 and 35 °C with Ce^{3+}, Mn^{2+}, and $Ru(bipy)_3^{2+}$ as catalysts. He pointed out that the complex BZ system behaves, in a sense, as if there is a single rate-determining step, since it obeys the Arrhenius equation, yielding practically the same activation energy for all three catalysts. In addition to experimentally confirming these striking findings, Blandamer et al.,[18,19] by systematically varying the rate constants in the model, identified the model step that most influences the frequency as the one representing the reaction between bromide and bromate ions to yield bromous acid. Misra[20] studied the BZ reaction both experimentally and numerically over a significantly wider temperature regime, from 30 to 90 °C, in a continuous-flow stirred tank reactor (CSTR). By using an extended Oregonator model that incorporates the bromination of malonic acid by hypobromous acid and bromine and the oxidation of malonic acid and its brominated derivatives by Ce^{4+} and other species to form bromide and free radicals, he demonstrated that the frequency cannot continue to grow exponentially without limit. Instead, with increasing temperature, oscillations disappear at a critical temperature via a Hopf bifurcation. Over this same range of temperatures, the amplitude of oscillations, however, remains essentially unchanged before quickly dropping near the bifurcation point. Similar conclusions were drawn by Strizhak and Didenko[21] for temperatures below 33 °C, employing the kinetic scheme of Györgyi and Field.[22]

None of the studies above, regardless of the model or scheme employed, examined the effects of varying the acidity or how the shape of the oscillations varies with temperature. Concentrations of reactants, except for sulfuric acid, were typically maintained in the range explored in the prior literature for the BZ reaction. Although increases in temperature did, as expected, shorten the period from typical values of ∼5 min to as low as 2 s,[20] one may wonder what range of frequencies is accessible to the BZ reaction. Use of alkylated species,[23,24] such as methylmalonic acid, or aromatic species,[25] such as pyrocatechol, as the substrate can lengthen the period by a factor of 10 or more. Might it be possible to *decrease* the period by several orders of magnitude, and could one model such high-frequency oscillations within the Oregonator framework? Here, we seek to answer these questions by exploring the uncharted regime of higher concentrations and temperatures, aiming to find high-frequency oscillations and to numerically reproduce, with a high degree of accuracy, the temperature dependence of the frequency and amplitude as well as the shape of oscillations with a four-variable Oregonator model. We also use the model to roam the reaction's phase space in search of even higher frequency oscillations in this well-studied chemical system.

Experimental Section

Oscillatory profiles are obtained by electrochemical measurements within the temperature range of 40−80 °C. Reaction mixtures are prepared from aqueous stock solutions of analytical-grade sodium bromate ($NaBrO_3$, Fisher), malonic acid ($CH_2(COOH)_2$, Sigma-Aldrich), sulfuric acid (H_2SO_4, Fisher, 5 M), and ceric ammonium nitrate ($(NH_4)_2Ce(NO_3)_6$, Fisher). The initial concentrations are $[NaBrO_3] = 0.5$ M, $[CH_2-$

* To whom correspondence should be addressed.
† Deceased, September 16, 2008. This paper is dedicated to the memory of Professor Anatol M. Zhabotinsky.

10.1021/jp901318z CCC: $40.75
Published on Web 04/17/2009

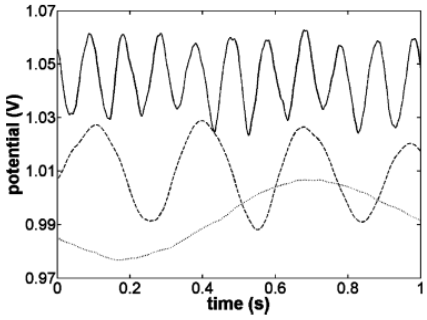

Figure 1. Oscillatory traces at three temperatures in the BZ reaction: 40 (dotted), 60 (dashed), and 80 °C (solid). Initial conditions are given in the Experimental Section. Profiles are shifted along the abscissa for clarity.

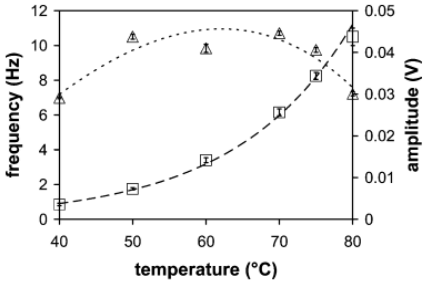

Figure 2. Initial oscillatory frequencies (squares) and amplitudes (triangles) in the temperature range 40−80 °C. Dashed line represents exponential curve fitted to experimental frequency data. Dotted line corresponds to the cubic curve drawn to aid the eye. Reactant concentrations are listed in the Experimental Section.

$(COOH)_2]$ = 2.0 M, $[H_2SO_4]$ = 1.5 M, $[(NH_4)_2Ce(NO_3)_6]$ = 1.0 mM, except where otherwise specified.

As the working electrode we use a glass-coated platinum wire with one end open to the electrolyte, immersed in 0.25 mL of BZ mixture held in a thin-walled 5 mm diameter glass tube. The working electrode potential is measured against a saturated calomel electrode (SCE, Fisher Scientific Accumet, gel filled) placed in a 1.5 cm diameter glass tube containing 0.25 M sodium sulfate (Na_2SO_4, Fisher) solution. Both half cells are submerged in a thermostat (Techne equipped with Techne TE-10D digital immersion circulator) and connected through a salt bridge, a 1 mm diameter glass U-tube filled with 0.25 M sodium sulfate in an agar−gel matrix (melting point ≈ 85 °C). Reaction mixtures are stirred with a 0.8 mm diameter glass rod attached to a high-rpm drill (Dremel 300). The potential difference is recorded with a high-performance USB acquisition module (Data Translation 9812) at sampling frequencies ranging from 100 to 1000 Hz. Despite the significant heat production, working with such small volumes of reaction mixture in the arrangement described above enables us to reliably keep the temperature within a ±1 °C range around its target value in the BZ half cell. Evaporation is negligible, as there is no discernible change in the height of the menisci, even at 80 °C. We are able to resolve oscillations with amplitudes of 10 mV and higher.

After lowering the fully assembled electrochemical cell into the water bath of the thermostat, we inject the requisite amounts of all preconditioned reagents, except the catalyst, into the BZ-batch half cell. Subsequently, under vigorous stirring, we add the catalyst to start the reaction.

Experimental Results

The preoscillatory induction period decreases with temperature, from about 300 s at 40 °C to about 30 s at 80 °C. During this portion of the reaction, the potential gradually decreases from its initial maximum value. This downward drift of the average potential continues throughout the oscillations and beyond, until the half-cell potential difference reaches zero. This effect can, however, be neglected within sufficiently short intervals.

Typical oscillatory profiles at several temperatures are shown in Figure 1. For better comparison, each is displaced along the time axis to fit within a 1 s interval. The profiles reveal the strong temperature dependence of the oscillatory frequency. The waveform is nearly sinusoidal between 40 and 80 °C, in contrast to the relaxation oscillations observed closer to room temperature. The data also show a small decrease in amplitude over the given temperature range.

In all cases, as the reaction proceeds, the frequency gradually decreases until oscillations finally cease with a period 20−30% longer than at the start. The number of cycles lessens with increasing temperature and drops to about 15 at 80 °C. The relative position of the curves along the ordinate suggests that the average potential rises with increasing temperature, though this conclusion is somewhat uncertain owing to small variations (<50 mV) from experiment to experiment in the overall potential differences between the BZ and SCE half cells.

Initial oscillatory frequencies and amplitudes for temperatures between 40 and 80 °C are presented in Figure 2. The frequency grows exponentially with temperature over the studied range, while the amplitude peaks at about 65 °C. The calculated activation energy is 58.0 ± 0.7 kJ/mol, in good agreement with previous studies.[17,19,26]

We also carried out experiments with 1,4-cyclohexanedione (CHD) as the organic substrate. In this set of experiments, ferroin is used as the catalyst and the traces are acquired spectrophotometrically. The maximum frequency of sinusoidal oscillations is measured to be 12 Hz with $[CHD]_0$ = 0.6 M, $[NaBrO_3]_0$ = 0.4 M, $[H_2SO_4]_0$ = 2.0 M, and [Ferroin] = 0.5 mM at 85 °C. We note that under such conditions we see surprisingly vigorous gas production in this reaction,[27] which is often regarded as a bubble-free BZ variant.

Model

The numerical analysis is based on a model incorporating all reactant species proposed by Zhabotinsky et al.[28] to describe the shape of oscillations and wave properties in the BZ reaction. The simplified set of equations used to describe our experimental findings is

$$dX/dt = -k_2h_0XY + k_3h_0AY - 2k_4'X^2 - k_5h_0AX + k_{-5}U^2 + k_6U(C-Z) - k_{-6}XZ \quad (1)$$

$$dY/dt = -k_2h_0XY - k_3h_0AY + qk_7BZ + k_9B \quad (2)$$

$$dZ/dt = k_6U(C-Z) - k_{-6}XZ - k_7BZ \quad (3)$$

$$dU/dt = 2k_5h_0AX - 2k_{-5}U^2 - k_6U(C-Z) + k_{-6}XZ \quad (4)$$

where $X = [HBrO_2]$, $Y = [Br^-]$, $Z = [Ce^{4+}]$, $U = [HBrO_2]$, h_0 is Hammet's acidity function,[29] $A = [NaBrO_3] = h_0/(0.2 + h_0)[NaBrO_3]_0$, $B = [MA]$, $C = [Ce^{3+}] + [Ce^{4+}]$, and $k_4' = k_4(1 + 0.87h_0)$. For numerical calculations, based on the initial reactant concentrations, we assign A_0 = 0.5 M, B_0 = 2 M, C = 0.001 M, and h_0 = 3, which corresponds to $[H_2SO_4]$ = 1.5 M. The

TABLE 1: Rate Parameters[a]

rate constant	20 °C	40 °C	ΔG [kJ/mol]	A[b]	80 °C	80 °C (this paper)
k_2 [M^{-2} s^{-1}]	7.57×10^6	1.2×10^7	15.0	1.24×10^7	2.60×10^7	4.95×10^7
k_3 [M^{-1} s^{-1}]	2.0	15	74.3	1.20×10^{11}	430	81.7
k_4 [M^{-2} s^{-1}]	8.6×10^3	1×10^4	3.23	111	1.3×10^4	2.5×10^4
k_5 [M^{-2} s^{-1}]	10	60	65.8	1.83×10^{10}	1187	3158
k_{-5} [M^{-1} s^{-1}]	4.2×10^6	6×10^6	11.1	1.35×10^6	1.1×10^7	2.1×10^7
k_6 [M^{-1} s^{-1}]	5×10^4	9×10^4	19.9	6.00×10^5	2.4×10^5	4.6×10^5
k_{-6} [M^{-1} s^{-1}]	5×10^4	2×10^4	5.99	798	3.7×10^4	6.95×10^4
k_7 [M^{-1} s^{-1}]	0.4	0.8	23.9	25.0	2.56	30.5
k_9 [s^{-1}]	3.3×10^{-6}	5×10^{-6}	13.3	2.67×10^{-6}	1.0×10^{-5}	2.4×10^{-5}

[a] Values in columns 2 and 3 are taken from ref 28. Values of the energy of activation ΔG in column 4 and the pre-exponential factor A in column 5 are computed from values of the rate constants in columns 2 and 3. Values in column 6 are obtained by extrapolation using values from columns 2 and 3. In column 7, values are adjusted to experiments at 80 °C. [b] Units are same as those for k_i.

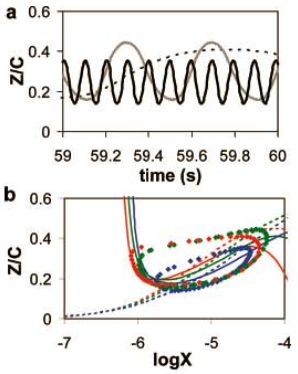

Figure 3. (a) Oscillatory solutions to systems 1−4 at $T = 80$ (black), 60 (gray), and 40 °C (dotted). $A_0 = 0.5$ M, $B = 2$ M, $h_0 = 3$ M, and $C = 0.001$ M. (b) Projections of limit cycles (composed of circles) on phase plane log X vs Z/C for temperatures $T = 80$ (blue), 60 (green), and 40 °C (red). Time elapsed between consecutive symbols: 5 ms. Solid and dashed lines are zero-growth isoclines (nullclines) for X and Z, respectively, calculated for the three temperatures. Note that the abscissa is logarithmic.

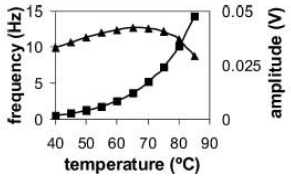

Figure 4. Simulated dependences of frequency (squares) and amplitude (triangles) of potential oscillations on temperature. Amplitude is calculated as $RT/F[\ln(Z_{max}/(C - Z_{max})) - \ln(Z_{min}/(C - Z_{min}))]$, where F is Faraday's constant. Parameter values are the same as in Figure 3.

stoichiometric parameter q is set to 0.6 in accordance with ref 28.

Numerical Results

Modeling our experimental findings requires rate constants applicable at high temperatures. For the reactions that lead to eqs 1−4, however, these quantities are available[28] only for 20 and 40 °C (Table 1, columns 2 and 3). To estimate their values at higher temperatures, we can use the absolute rate theory, according to the which a rate constant can be calculated as $k(T) = AT \exp(-E_a/RT)$, where k, A, T, and E_a are the rate constant, pre-exponential factor, absolute temperature, and activation energy, respectively. For the rate constant values given by this formula (listed in column 6 of Table 1), oscillations vanish at temperatures as low as 55 °C with frequencies below 1 Hz at the Hopf bifurcation. In our experiments, however, we observe oscillations at 60 °C (~3 Hz) and higher temperatures.

To address this discrepancy and to quantitatively capture the experimentally observed oscillations, we adjusted all rate constants to obtain the best fit with the experimental data, specifically the frequency and amplitude of oscillations at 80 °C for $A_0 = 0.5$ M, $B_0 = 2$ M, $C = 0.001$ M, and $h_0 = 3$ and the concentration of bromate A_0 at which the Hopf bifurcations at 40 and 60 °C occur for $B_0 = 2$ M, $C = 0.001$ M, and $h_0 = 3$ (Figure 5a). We chose the bromate vs temperature phase diagram (Figure 5a) because the system is quite sensitive to changes in the bromate concentration. We believe that this approach is more reliable than simply fitting potential time series because the fast oscillations last only a few seconds.

Comparing the resulting constants (column 7) to their counterparts given by the absolute rate theory (column 6), we find that only the differences in the k_3 and k_7 values (rows 3 and 9) are significant. These steps correspond, respectively, to the following reactions

$$H^+ + Br^- + HBrO_3 \leftrightarrow HBrO_2 + HOBr \quad (5)$$

$$Ce^{4+} + CHBr(COOH)_2 \leftrightarrow Ce^{3+} + CBr(COOH)_2^{\bullet} + H^+ \quad (6)$$

Reaction 5 was identified by Blandamer at al.[19] as the major determinant of the oscillatory frequency, and its activation energy was measured to be 54 kJ/mol.[30] Substituting this value and the corresponding rate constant at 20 °C (Column 2) into the absolute rate theory equation yields a rate constant of 86.6 M^{-1} s^{-1} at 80 °C, which is in excellent agreement with that calculated in this study. The activation energy of reaction 6 is reported to be 67 kJ/mol[21] and is assumed to be close to the total energy of activation,[31] which is 58 kJ/mol. With the extrapolation method, these two values of E_a both yield fairly good estimates for k_7, 42.9 and 22.9 M^{-1} s^{-1}, respectively. Hence, we conclude that our corrections for constants k_3 and k_7 are reasonable and consistent with literature data.

With these adjustments to the rate constants, the calculated frequencies, amplitudes, and shapes of the oscillatory profiles faithfully reflect our experimental findings (see Figure 3a). Analyzing the dynamics of the four-variable model on the phase plane provides detailed insights into the behavior of the BZ reaction at elevated temperatures. According to Figure 3b, the limit cycle is fairly symmetric for all three temperatures, which is consistent with the sinusoidal character of the oscillatory traces. As the temperature is increased, the limit cycle shrinks and the oscillations become substantially faster. The distance

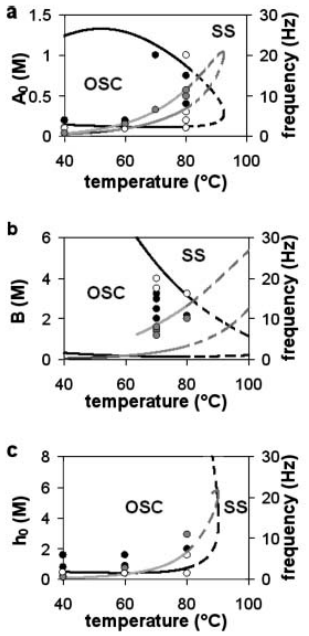

Figure 5. Calculated parametric diagrams $T-A_0$ (a), $T-B$ (b), and $T-h_0$ (c). Remaining parameters are the same as in Figure 1. Black lines indicate boundaries between dynamic states. Symbols OSC and SS denote areas corresponding to oscillation and stationary states, respectively. The secondary ordinate axis shows the oscillation frequency (gray lines) at Hopf bifurcation points. Circles correspond to experimental results: no oscillations (empty circles), oscillations (solid back circles), with frequencies shown by solid gray circles.

between the extrema of Z, however, changes much less rapidly, which translates to oscillations with nearly constant amplitude throughout the studied temperature regime, as observed in experiment and previously reported for dilute BZ mixtures.[20]

The oscillatory frequency and amplitude dependence on temperature obtained from the model are presented in Figure 4. As in the experiments, there is an exponential relationship between frequency and temperature. The calculated amplitude exhibits the same tendencies seen in the experiments (Figure 2). Compared to the frequency, the amplitude remains within a narrow range, first growing, then passing through a maximum, and finally decreasing as the temperature approaches 80 °C. Simulations suggest that the sharp fall in amplitude continues while the frequency rapidly increases until oscillations finally disappear around 90 °C with a frequency of about 20 Hz. Spectrophotometric measurements at higher temperatures with ferroin as catalyst using slightly different reactant concentrations support this prediction. The oscillatory regime in these ferroin-catalyzed experiments extends above 80 °C, and the frequency can reach as high as 18 Hz for temperatures near 100 °C.

The fitted total activation energy is 68.2 ± 0.1 kJ/mol, which exceeds that found in experiment. This difference is a consequence of the tendency of the model to underestimate frequencies for lower temperatures, as it is primarily designed to accurately describe the high-frequency oscillations.

Our model, despite the aforementioned weakness, enables us to numerically explore the high-frequency oscillatory regime of the BZ system. When mapping this domain of the reaction's phase space, we keep all but one parameter as well as the total catalyst concentration constant while systematically changing the remaining parameter and the temperature. Guided by the numerical results, we carry out experiments along sections of the calculated boundaries separating oscillatory and stationary regimes to test the model over a broader domain in the phase space. The resulting parametric diagrams (see Figure 5) demonstrate that our model largely reflects the empirical findings. Boundaries and frequencies are in good agreement with the experimental data, though in a few cases, typically at high temperatures, the oscillatory domains are narrower than predicted by the model. This discrepancy may result, at least in part, from the sharp drop in amplitude that occurs near the Hopf bifurcation, which leads to oscillations that we cannot resolve experimentally. Simplifications in the model that reduce the complexity of the system may also lead to quantitative mismatches between experiment and simulation. The approximate calculation of hydronium ion concentrations, especially at high temperatures, is another factor likely to reduce the accuracy of the model. Looking at Figure 5, however, we conclude that the four-variable model renders all dynamical aspects of the high-temperature reaction rather well. Consequently, we can make calculations with some confidence up to 100 °C to further explore the phase space. The dashed lines show the likely characteristics of the reaction at temperatures near the normal boiling point of water. It seems probable that, by decreasing the malonic acid concentration while keeping the others constant, one could reach ~25 Hz oscillations near 100 °C.

Conclusions

Our experimental results show that chemical systems such as the Belousov−Zhabotinsky reaction can support oscillations with frequencies above 10 Hz. We demonstrated that this frequency regime is easily accessible and studying it requires no special equipment. High-frequency oscillations can, however, be sustained only for a few seconds in closed systems, though they should continue indefinitely in a flow reactor.

Numerical simulations show that our four-variable model quantitatively describes all dynamical features of the reaction between 40 and 80 °C. This allowed us to map the phase space at higher temperatures and identify possible pathways leading to frequencies approaching 25 Hz. These experiments would require a sealed tube to avoid evaporation, a stir bar instead of a glass rod immersed in the reaction mixture from above, and perhaps a high-performance temperature control system able to compensate for the rapid heat production.

In a high-pressure environment, it might be possible to exceed significantly even the 3−4 orders of magnitude increase we achieved here over the typical BZ oscillation frequency. In principle, the temperature could be increased to the critical point of water (374 °C) while maintaining oscillations, though other factors, including the increased dissociation of water and the decarboxylation of malonic acid, would have to be taken into account. It would perhaps be worthwhile to make calculations using our model to estimate a feasible frequency limit that could be reached experimentally if one were interested in increasing the speed of chemical computation devices[32] that incorporate BZ oscillators.

Acknowledgment. We thank the National Science Foundation (grant CHE-0615507) and the Defense Advanced Research Projects Agency for support.

References and Notes

(1) Belousov, B. P. *Sb. Ref. Radiats. Med.*; Medgiz: Moscow, 1958; p 145.

(2) Zhabotinsky, A. M. *Biofizika* **1964**, *9*, 306.
(3) Field, R. J.; Körös, E.; Noyes, R. M. *J. Am. Chem. Soc.* **1972**, *94*, 8649.
(4) Field, R. J.; Noyes, R. M. *J. Chem. Phys.* **1974**, *60*, 1877.
(5) Field, R. J.; Noyes, R. M. *Faraday Symp. Chem. Soc.* **1974**, *9*, 21.
(6) Ruoff, P. *Chem. Phys. Lett.* **1982**, *72*, 76.
(7) Geiseler, W.; Föllner, H. H. *Biophys. Chem.* **1977**, *6*, 107.
(8) Ruoff, P. *J. Phys. Chem.* **1993**, *97*, 6405.
(9) Epstein, I. R. *Nature (London)* **1995**, *374*, 321.
(10) Richetti, P.; Roux, J. C.; Argoul, F.; Arneodo, A. *J. Chem. Phys.* **1987**, *86*, 3339.
(11) Argoul, F.; Arneodo, A.; Richetti, P.; Roux, J. C.; Swinney, H. L. *Acc. Chem. Res.* **1987**, *20*, 436.
(12) Armstrong, G. R.; Taylor, A.; Scott, S. K.; Gáspár, V. *Phys. Chem. Chem. Phys.* **2004**, *6*, 4677.
(13) Zaikin, A. N.; Zhabotinsky, A. M. *Nature (London)* **1970**, *225*, 535.
(14) Winfree, A. T. *Science* **1972**, *175*, 634.
(15) Alonso, S.; Sagués, F.; Mikhailov, A. S. *J. Phys. Chem. A* **2006**, *110*, 12063.
(16) Luengviriya, C.; Hauser, M. J. B. *Phys. Rev. E* **2008**, *77*, 056214.
(17) Körös, E. *Nature (London)* **1974**, *251*, 703.
(18) Blandamer, M. J.; Morris, S. H. *J. Chem. Soc., Faraday Trans* **1975**, *I 71*, 2319.
(19) Blandamer, M. J.; Roberts, D. L. *J. Chem. Soc., Faraday Trans* **1977**, *73*, 1056.
(20) Misra, G. P. *Chem. Phys. Lett.* **1992**, *191*, 435.
(21) Strizhak, P. E.; Didenko, O. Z. *Theor. Exp. Chem.* **1997**, *33*, 133.
(22) Györgyi, L.; Field, R. J. *J. Phys. Chem.* **1991**, *95*, 6594.
(23) Ruoff, P.; Schwitters, B. *Z. Phys. Chem.-Wiesbaden* **1982**, *132*, 125.
(24) Chen, Y. F.; Lin, H. P.; Sun, S. S.; Jwo, J. J. *Int. J. Chem. Kinet.* **1996**, *28*, 345.
(25) Harati, M. Ph.D. thesis, University of Windsor, 2008.
(26) Nagy, G.; Körös, E.; Oftedal, N.; Tjelflaat, K.; Ruoff, P. *Chem. Phys. Lett.* **1996**, *250*, 255.
(27) Farage, V. J.; Janjic, D. *Chem. Phys. Lett.* **1982**, *88*, 301.
(28) Zhabotinsky, A. M.; Buchholtz, F.; Kiyatkin, A. B.; Epstein, I. R. *J. Phys. Chem.* **1993**, *97*, 7578.
(29) Hammett, L. P.; Deyrup, A. J. *J. Am. Chem. Soc.* **1932**, *54*, 2721.
(30) Kshirsagar, G.; Field, R. J. *J. Phys. Chem.* **1988**, *92*, 7074.
(31) Ruoff, P. *Physica D* **1995**, *84*, 204.
(32) Adamatzky, A. *Computing in Nonlinear Media and Automata Collectives*; IOP: London, 2001.

JP901318Z

THE JOURNAL OF PHYSICAL CHEMISTRY Letters

pubs.acs.org/JPCL

Synchronization of Chemical Micro-oscillators

Masahiro Toiya,[†,§,∥] Hector O. González-Ochoa,[‡,∥] Vladimir K. Vanag,[†] Seth Fraden,[‡] and Irving R. Epstein*[,†]

[†]Department of Chemistry, Brandeis University, Waltham, Massachusetts 02454, [‡]Department of Physics, Brandeis University, Waltham, Massachusetts 02454, and [§]CCS Inc., Burlington, Massachusetts 01803

ABSTRACT Many phenomena of biological, physical, and chemical importance involve synchronization of oscillatory elements. We explore here, in several geometries, the behavior of diffusively coupled, nanoliter volume, aqueous drops separated by oil gaps and containing the reactants of the oscillatory Belousov−Zhabotinsky (BZ) reaction. A variety of synchronous regimes are found, including in- and antiphase oscillations, stationary Turing patterns, and more complex combinations of stationary and oscillatory BZ drops, including three-phase patterns. A model consisting of ordinary differential equations based on a simplified description of the BZ chemistry and diffusion of messenger (primarily inhibitory) species qualitatively reproduces most of the experimental results.

SECTION Kinetics, Spectroscopy

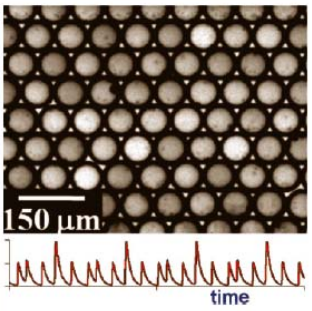

Studies of synchronized oscillators have generated significant insights into a diverse array of physical, chemical, and biological phenomena since the first known efforts by Huygens in the seventeenth century.[1] In biology, coupled oscillator approaches have been applied, for example, in modeling the growth of slime molds,[2] bimanual coordination of vertebrates,[3−5] and in much more complex simulations of the human brain.[6] The coupling can be local or global (e.g., all-to-all) or a combination,[7,8] as well as attractive (excitatory) or repulsive (inhibitory). Global inhibitory coupling in chemical or electrochemical oscillatory systems led to the discovery of such new patterns as oscillatory or chaotic clusters.[9,10] Global excitatory coupling usually results in system-wide in-phase synchronization (above a critical value of the coupling strength).[11] When the coupling is purely excitatory or when excitatory coupling is dominant,[12,13] a system typically has two states: asynchronous, in which the oscillators have random phases, and synchronous, when all oscillators are in-phase with one another. Time delays associated with the coupling can complicate this simplified picture.

Local inhibitory coupling has been much less investigated experimentally, though it is found in many important cases. Examples of inhibitory coupling include interneuron communication in the brain[6] and coupled semiconductor lasers.[14] Several theoretical works suggest that inhibitory coupling should produce many different synchronous regimes and multistability between them.[15−19] Recently, we developed an experimental system consisting of a linear array of small (50−300 μm in diameter) identical water droplets separated by oil gaps.[20] Each drop contains the reactants of the oscillatory Belousov−Zhabotinsky (BZ) reaction:[21,22] malonic acid (MA), bromate, sulfuric acid, ferroin (catalyst), and a small amount of $Ru(bpy)_3$, which serves both as a cocatalyst and to make the BZ reaction photosensitive. Droplets are diffusively coupled through the inhibitor, Br_2, which preferentially dissolves in the oil gaps. We observed antiphase synchronization and stationary Turing patterns in this system.[20]

In this letter we report new synchronized patterns observed in two-dimensional (2D) arrays of oscillatory BZ microdrops, as well as novel, more complex patterns found in linear (1D) configurations and in arrays of partially stacked ("1.5D") drops. Thus we experimentally confirm that inhibitory coupling is able to produce a rich variety of patterns.

In the 1D configuration, the most stable behavior is the previously reported antiphase oscillation,[20] in which each drop is 180° out of phase with its neighbors. If we synchronize the drops initially with a flash of light and block communication between drops by adding a bromine scavenger to the oil between drops (see Supporting Information, Methods), then we initially observe in-phase synchronization, but, because there are small differences in frequency between the drops, this regime demonstrates a slow phase drift that soon destroys the synchrony. If no scavenger is employed, the drops remain in phase for tens of oscillations, indicating active in-phase synchronization (see Supporting Information, Figure S1). Our simulations show, however, that in-phase synchronization with inhibitory coupling has a much smaller basin of attraction than antiphase synchronization. Experimentally, delaying the phase of a single drop in a synchronized in-phase 1D arrangement with a focused laser beam initiates a transition to an antiphase pattern that propagates out from the delayed drop. Indeed, a quite precise in-phase initial condition among all drops is necessary to produce in-phase synchronization.

In the 1.5D experiments, when the drop diameter lies between $0.5d$ and d, where d is the inner diameter of the glass

Received Date: February 19, 2010
Accepted Date: March 18, 2010

DOI: 10.1021/jz100238u | *J. Phys. Chem. Lett.* **2010**, *1*, 1241–1246

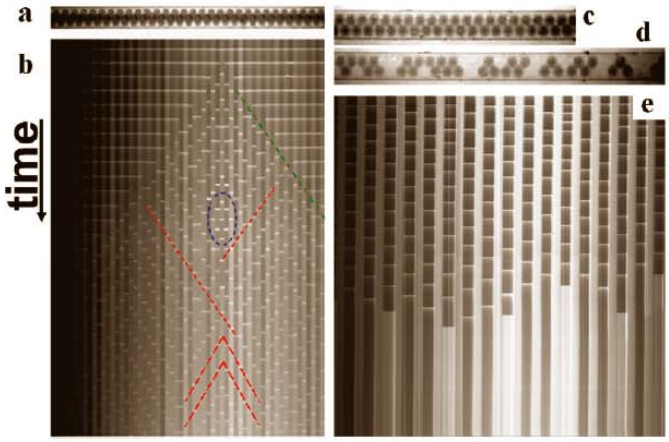

Figure 1. Snapshots (a,c,d) and space-time plots (b), (e, 1D) of patterns emerging from initially in-phase arrays of partially stacked (1.5D) BZ drops in a 150 μm ID capillary. In frames b and e, spikes of oxidation of ferroin are seen as short horizontal light lines (flashes) across BZ-drops. In frames a and b, horizontal length of the frame is 3.8 mm; total time shown in b is 3900 s. In frames c, d, and e, horizontal lengths are 1.6, 2.2, and 4.6 mm, respectively. Total time shown in e is 12 000 s. Initial concentrations of reactants: $[H_2SO_4]$ = 0.08 M, $[NaBrO_3]$ = 0.288 M, [MA] = 0.64 M (a, b), 0.040 M (c−e), [NaBr] = 10 mM, [ferroin] = 3 mM, and $[Ru(bpy)_3]$ = 0.4 mM (bpy = bipyridine).

capillary, the drops self-organize to form a zigzag structure (Figure 1a). This geometry, in which each drop has four neighbors, two near and two more distant, produces a wealth of new stable patterns, some of which are shown in Figures 1 and 2. The space−time plots consist of the intensity taken along a horizontal line through the center of the capillary as a function of time. In Figure 1b we follow the evolution of 60 drops in one very complex regime, in which all the drops oscillate. Initially, all drops are in-phase, but in the second cycle shown, drop 38 (numbering starts from the left) experiences a delay in flashing. This phase shift cascades to the neighboring drops, generating a switching wave shown by the green dotted lines. The velocity of this wave is about 0.8 μm/s, approximately equal to the linear size of a drop divided by the period of oscillation. Note, however, that the oscillation period can vary significantly depending on the synchronous regime. For example, the period of the initial in-phase regime is much shorter than that of the final staggered pattern. The same behavior emerges in the simulations.

Looking carefully at Figure 1b, we see that the drops near drop 38 oscillate 180° out-of-phase with their neighbors. A typical stretch of out-of-phase behavior is marked by the blue oval. Other sets of neighboring drops assume phase differences close to ±120°, as highlighted by red dashed lines in Figure 1b. There are also several pairs of neighboring drops that oscillate in-phase from time to time. A simpler behavior in 1.5D, stationary Turing patterns found at a lower MA concentration, is illustrated in Figure 1c,d,e. In the experiment shown in Figure 1c,d, all drops initially oscillate in-phase after a brief synchronizing illumination (Figure 1c). Soon, each drop ceases to oscillate and reaches a stationary reduced or oxidized state, forming the Turing structure (Figure 1d). The characteristic length of this pattern is several drops, suggesting that the Turing wavelength can be larger, perhaps much larger, than the distance between neighboring drops. The dynamics of an array of drops in a 1D chain that ultimately reaches a stationary and more regular Turing pattern obtained in another experiment is shown in Figure 1e. Here, the characteristic length of the pattern comprises exactly two drops in a reduced state and one drop in an oxidized state. Note that before the system reaches the stationary Turing regime, the drops oscillate antiphase.

Figure 2 demonstrates a novel pattern found in the 1.5D geometry, where all drops in one row (see Figure 2a,d) are stationary, while drops in the other row oscillate antiphase. Figure 2b shows the initial stage of these oscillations, and Figure 2c shows the final stable regime. These drops were not initially synchronized, as no $Ru(bpy)_3$ was added to this system, so the drops begin to oscillate with random phases (Figure 2b). A schematic representation of the pattern behavior is shown in Figure 2d: drops in the bottom row (represented as blue or red) oscillate antiphase, while drops in the upper row remain in a stationary reduced state (gray). The spatial period of this pattern consists of four drops. This pattern is neither a Turing pattern nor a simple antiphase oscillatory pattern. It is difficult to identify an analogous behavior in the homogeneous spatially extended reaction−diffusion system, although if we equate stationary drops to nodes, then this pattern might be thought of as a discrete analog of a standing wave. Another possible analogy is to the oscillatory out-of-phase Turing patterns found recently.[23,24]

In 2D geometry, the drops, when packed at high density, spontaneously form a hexagonal array. The regime consisting of antiphase oscillation between all neighboring pairs, which is extremely stable in the 1D geometry, is impossible in a hexagonal 2D geometry. A similar, symmetry-generated situation arises in an analogous Hamiltonian system: the 2D antiferromagnetic XY model.[25,26] To resolve this geometrical constraint, our drops respond in different ways. Figure 3a shows a pattern, denoted "π-S", in which stationary drops

DOI: 10.1021/jz100238u | J. Phys. Chem. Lett. 2010, 1, 1241–1246

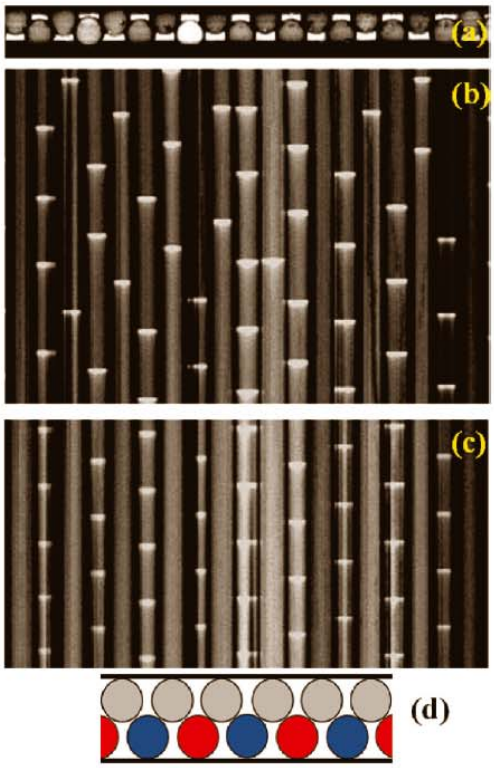

Figure 2. Pattern consisting of stationary and antiphase oscillatory BZ drops in 1.5D geometry. (a) Snapshot of capillary with BZ drops; (b,c) space−time plots (time-axis is vertical) for (b) early times during transient period and (c) later, after the stationary regime is established; (d) schematic representation of the pattern. Initial concentrations of BZ reagents are as in Figure 1 with [MA] = 0.64 M, except [Ru(bpy)$_3$] = 0. Drop size is 65 μm. Oscillation period is 177 s. Length of frames is 1.044 mm. Times shown in frames b and c are 1068 and 798 s, respectively.

(black) surrounded by six oscillating antiphase drops form a larger hexagonal pattern. Figure 3b shows this pattern schematically, with stationary drops in gray, and blue and red drops oscillating out of phase by nearly 180°. As a result, drop 10 (or drops 2, 4, 7, 13, 16, 18, etc.) in Figure 3b is exposed to inhibitory bromine signals twice as often as any of the red−blue pairs. This inhibition is apparently sufficient to prevent it from oscillating, pushing it into a stationary reduced state. This 2D pattern bears similarities to the mixed stationary−oscillatory 1.5D pattern shown in Figure 2; however, the spatial period of the pattern in Figure 3 taken along any of the three hexagonal axes consists of three drops. Figure 3c,d shows space−time plots for selected drops, confirming the antiphase behavior of neighboring drops.

A second configuration for drops in 2D, denoted "2π/3," is shown in Figure 4, where the neighboring drops oscillate with a phase shift close to 120°, corresponding to the ground state of the 2D antiferromagnetic XY model.[25,26] A snapshot of the system is shown in Figure 4e, with the outlined region

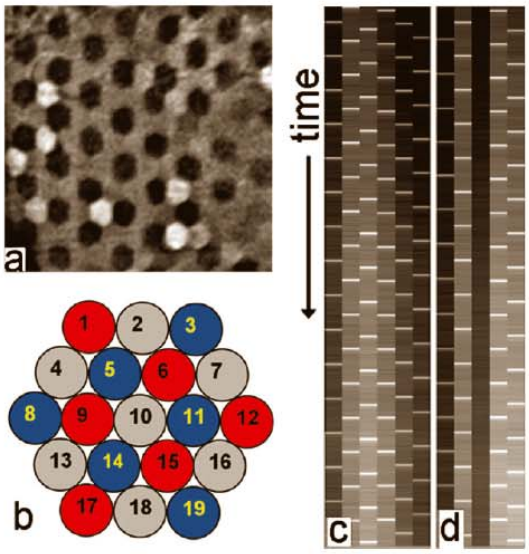

Figure 3. Stationary and antiphase oscillatory BZ drops in 2D. (a) Hexagonally packed drops forming a larger hexagon with each stationary drop (black) surrounded by six oscillatory drops. Imaged area is 0.7 × 0.7 mm. (b) Schematic representation of the pattern (stationary drops in gray). (c,d) Space−time plots (duration 2800 s) of drops 6, 11, 15, 14, 9, and 5 (c) and drops 1, 5, 10, 15, and 19 (d). Concentrations of BZ reagents are as in Figure 1.

of interest magnified in Figure 4f. Frames a−d are snapshots of the region centered around drop 1 in Figure 4f taken after the stationary behavior has been reached. The interval between snapshots is about 73 s, i.e., 1/3 of the single drop oscillation period of 220 s. Drops 2, 4, and 6 oxidize in-phase in frame a, followed by in-phase oxidation of drop 1 and its symmetrically equivalent counterparts (b), and finally drops 3, 5, and 7 (c). The cycle starts again in frame (d). Figure 4g shows a staggered space−time plot of drops 1−7, marked in (f). This regime resembles the portions of Figure 1b with phase shift $\cong$ 120° between neighboring drops. The most important difference between the conditions that result in the two patterns illustrated in Figure 3 (π-S) and Figure 4 (2π/3) is that π-S patterns are obtained at stronger coupling, which we can characterize by the dimensionless ratio $D/(kL^2)$. Here D is the effective diffusion coefficient of the inhibitor (bromine), k is the effective (first-order) rate constant for the consumption of the inhibitor, and L is the distance between drops. There are at least two ways to increase the coupling strength: (*i*) by decreasing the size of the water droplets or (*ii*) by decreasing the length of the oil gap between droplets. We explored both methods (to decrease the oil gap, we decreased the amount of oil in the emulsion). With either method, an increase in coupling strength (e.g., by decreasing the droplet diameter from 120 to 90 μm) leads to a transition from the 2π/3 to the π-S pattern. More generally, stronger coupling results in a higher proportion of stationary droplets, a result found in both the experiments and the simulations. The simulations

DOI: 10.1021/jz100238u | J. Phys. Chem. Lett. 2010, 1, 1241–1246

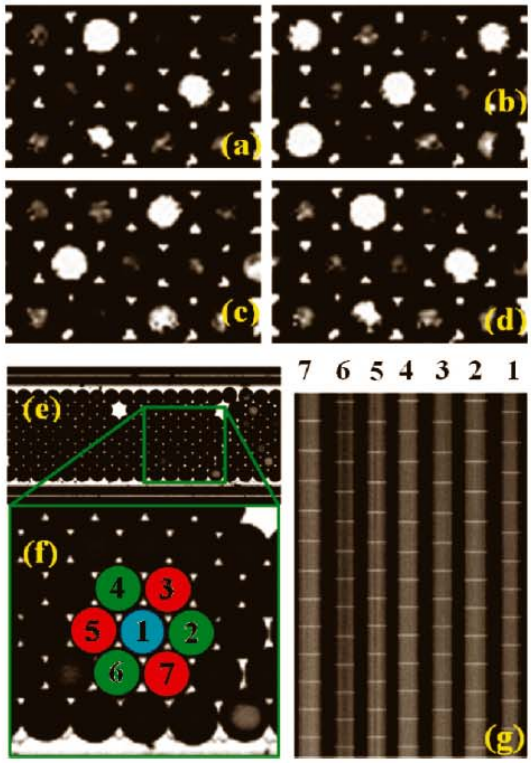

Figure 4. Three-phase oscillatory clusters in 2D. Drop diameter is 128 μm. Initial concentrations: $[H_2SO_4]$ = 0.08 M, $[NaBrO_3]$ = 0.29 M, [MA] = 0.64 M, [Ferroin] = 3 mM, [NaBr] = 0.01 M, and $[Ru(bpy)_3]$ = 1.2 mM. Snapshots a−d are taken at t = 0, $T/3$, $2T/3$, and T, where $T \cong 231$ s. Snapshot e and its enlargement (f) show a 2D configuration of BZ drops. (g) Space−time plot for drops 1−7 shown in snapshot f; dimensions are 896 μm horizontal and 2877 s vertical. Period of oscillations for each drop in the space−time plot is the same as T in snapshots a−d.

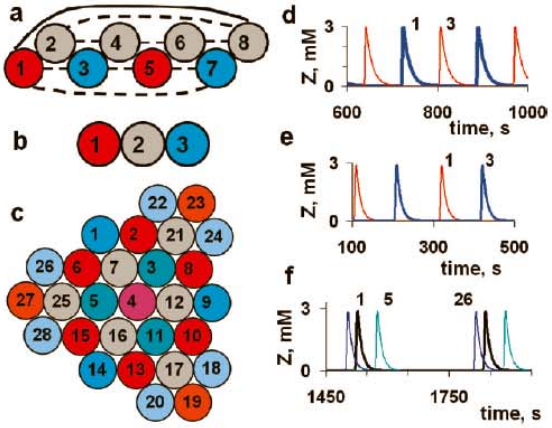

Figure 5. Simulations. (a,d) Eight identical coupled BZ drops for 1.5 D configuration. (a) Gray drops are stationary. Drops 1 and 5 oscillate in-phase, drops 3 and 7 also oscillate in-phase but antiphase to drops 1 and 5. (d) Oscillations of drops 1 and 3, T = 165.5 s, z is the oxidized form of the catalyst. Chemical parameters: $h = [H^+]$ = 0.2 M, $a = [BrO_3^-]$ = 0.3 M, m = [MA] = 0.5 M, c_0 (total concentration of the catalyst) = 0.003 M. Coupling parameters: k_f (coupling strength between close droplets like 1 and 2) = 1 s^{-1}, $1/k_b$ (associated with time delay in coupling) = $P_B/\rho_V k_f$, P_B (partition coefficient for Br_2 between water and oil) = 2.5, ρ_V (volume ratio of water drops and oil gaps) = 10, k_{fd} (coupling strength between distant droplets like 1 and 3 in frame a) = $k_f/10$, $\rho_{V2} = 2$, $k_{bd} = \rho_{V2} k_{fd}/P_B$, $k_O = k_{fr} = 0$. (b,e) The minimum number (three) of drops simulating the pattern in Figure 3. The gray drop is stationary. Drops 1 and 3 oscillate antiphase, as shown in frame e. Parameters: h = 0.16 M, a = 0.3 M, m = 0.65 M, k_f = 1 s^{-1}, P_B = 2.5, ρ_{V2} = 10. (c,f) Twenty-eight identical hexagonally packed BZ drops. (c) Gray drops (7, 21, 12, 25, 16, and 17) are in the oxidized SS (oscillates with very small amplitude). Reddish drops oscillate almost in-phase. Bluish drops also oscillate almost in-phase and antiphase to reddish drops. (e) phase shift between three types (with slightly different environments) of bluish drops (1, 5, and 26). Parameters: as in (b,e) except k_f = 0.4 s^{-1}. Other constants used in the FKN model S1−S12 are specified in the caption for Figure 3S in the Supporting Information.

further suggest that, in the limit of very strong coupling, a limit we have achieved in the 1D but not in the 2D experiments, all droplets become stationary, resulting in Turing patterns. At intermediate coupling strengths, the slightly different initial conditions may also contribute to the selection of different final patterns by our system. In both cases, we have patterns consisting of three groups of droplets having either different phases or different dynamical behavior (stationary or oscillatory drops).

To better understand our experimental results, we carried out computer simulations on a simplified model of our system S1−S12, described in the Supporting Information, Modeling. Because, even at this level of simplification, modeling large arrays of drops is computationally taxing, we explored mainly configurations consisting of small numbers of drops to see whether the key features of our 1D, 1.5D, and 2D systems would emerge.

Typical results of simulations are shown in Figure 5. The regime seen in Figure 2 with stationary and antiphase oscillatory BZ drops is reproduced in Figure 5a,d for an eight-drop array in the 1.5D configuration. Stationary Turing patterns resembling the experimental patterns shown in Figure 1d,e are presented in the Supporting Information, Results (Figure S3). Such Turing patterns are obtained with stronger inhibitory coupling (through bromine) and/or at smaller concentrations of MA, as in the experiments. Note that a decrease in [MA] leads to higher $[Br_2]$ in the drops and the intervening oil and consequently gives stronger inhibitory coupling.

The 2D pattern shown in Figure 3 can be simulated with an array of three linearly coupled drops in 1D shown in Figure 5b,e (where the central drop is nearly stationary and the two end drops oscillate antiphase, over a broad range of concentrations) and several configurations of hexagonally packed drops shown in Figure 5c. For example, if we take only drops 1−7 as labeled in Figure 5c, drops 1−12, 1−16, 1−20, or 1−24, we obtain patterns as in Figure 3. However, if the number of drops in our cluster is small (less than about 20), the final pattern is very sensitive to the addition or removal of a single droplet. A cluster of 28 drops (shown in Figure 5c) is much less sensitive to this procedure. A number of

DOI: 10.1021/jz100238u | J. Phys. Chem. Lett. 2010, 1, 1241–1246

questions about the sensitivity of the pattern to the number of droplets, the coupling strength, the symmetry of the droplet configuration, and the initial conditions remain. Note that droplets that oscillate "in-phase," like the reddish or bluish droplets in Figure 5c, have a slight phase shift, as shown in Figure 5f. An analogous phase shift can be seen in all our experimental results. The origin of this shift in the simulations is the different number of neighbors for boundary and "inner" droplets.

The three-phase oscillatory patterns shown in Figure 4 can be simulated with just three circularly coupled BZ drops plus three oil drops (like drops 1, 2, and 7 in Figure 5c, for example; see also Supporting Information, Results, Figure S4). Curiously, the three-phase pattern of Figure 3 cannot be modeled with three circularly coupled drops. Both of the two three-phase patterns in 2D, π-S and $2\pi/3$, are found in a cluster of six identical drops connected in 3D to form an octahedron (Supporting Information, Results, Figure S5). This unique configuration allows us to have periodic boundary conditions, an even number of neighbors (4 vs 6 in hexagons), and a total number of drops divisible by 3 (the spatial period for these two patterns). Simulations reveal that an increase in coupling strength leads to a transition from $2\pi/3$ to π-S patterns, just as we observe in our experiments. However, there is no clear physical correspondence between the experimental configuration of hexagonally packed drops and the simulations on 3D octahedrons.

In our simulations, we used the well-known FKN mechanism for the BZ reaction,[27] in which $BrO_2^{\bullet}$ radical serves as an excitatory messenger between droplets, and Br_2 acts as an inhibitory messenger. Excluding $BrO_2^{\bullet}$ as a messenger in the model causes almost no change in the calculated patterns, which suggests that this species plays practically no role in the coupling.

The formation of two-phase and three-phase structures, i.e., sets of drops that oscillate with a common phase (or are stationary) in our system, may be viewed as a generalization of the chemical quorum sensing recently reported[13] in sets of particles loaded with catalyst and immersed in a BZ solution. Here, too, the individual drops behave independently until brought together so that their density (or coupling strength) exceeds a critical value. They then begin to exhibit more complex dynamical behavior, in our case antiphase and three-phase patterns as well as the in-phase oscillation observed in the particle experiments. Our oscillatory structures also resemble the clusters observed in experiments on globally coupled electrochemical oscillators.[10] The larger the coupling strength, the larger the number of different synchronous groups (up to the limit of Turing patterns). Therefore in addition to the "quorum sensing", our system exhibits a primitive kind of "differentiation".

Since the coupling of our oscillatory BZ drops is primarily inhibitory, and they can form stationary Turing-like patterns (if the coupling is strong enough), this system can be viewed as a discrete manifestation of the Turing−Hopf interaction that generates many interesting patterns in continuous reaction-diffusion systems, such as oscillatory in-phase and antiphase Turing patterns (the latter is analogous to our antiphase regime).[23,24]

All configurations that we have studied computationally demonstrate multiple synchronous regimes, i.e., regimes in which each drop has the same total period (though possibly with different numbers of maxima during this period). We expect to find some of these regimes in further experiments on our system of coupled BZ droplets, which mimics diffusive inhibitory coupling among biological objects, a situation that is ubiquitous in nature.

SUPPORTING INFORMATION AVAILABLE

Methods, modeling, and results as Figures S1−S5. This material is available free of charge via the Internet at http://pubs.acs.org.

AUTHOR INFORMATION

Corresponding Author:

*To whom correspondence should be addressed. E-mail: epstein@brandeis.edu.

Author Contributions:

‖ These authors contributed equally to this work.

ACKNOWLEDGMENT

This work was supported by the National Science Foundation (CHE-0615507 and MRSEC DMR-0820492) and by the Defense Advanced Research Projects Agency. M.T. and I.R.E. thank Milos Dolnik and the late Anatol Zhabotinsky for helpful comments and suggestions. We thank CCS Inc. for providing the LED illuminator used in some of the experiments in this work.

REFERENCES

(1) Strogatz, S. H. *SYNC: The Emerging Science of Spontaneous Order*; Hyperion: New York, 2003.
(2) Saigusa, T.; Tero, A.; Nakagaki, T.; Kuramoto, Y. Amoebae Anticipate Periodic Events. *Phys. Rev. Lett.* **2008**, *100*, 018101.
(3) Grossberg, S.; Pribe, C.; Cohen, M. A. Neural Control of Interlimb Oscillations 0.1. Human Bimanual Coordination. *Biol. Cybern.* **1997**, *77*, 131–140.
(4) Butt, S. J. B.; Lebret, J. M.; Kiehn, O. Organization of Left−Right Coordination in the Mammalian Locomotor Network. *Brain Res. Rev.* **2002**, *40*, 107–117.
(5) Uematsu, K.; Baba, Y.; Kake, Y.; Ikenaga, T.; Moon, S. J.; Yoshida, M. Central Mechanisms Underlying Fish Swimming. *Brain Behav. Evol.* **2007**, *69*, 142–150.
(6) Izhikevich, E. M. *Dynamical Systems in Neuroscience: The Geometry of Excitability and Bursting*; MIT Press: Cambridge, MA, 2007.
(7) Pikovsky, A.; Rosenblum, M.; Kurths, J. *Synchronization. A Universal Concept in Nonlinear Sciences*; University Press: Cambridge, U.K., 2001.
(8) Abrams, D. M.; Strogatz, S. H. Chimera States for Coupled Oscillators. *Phys. Rev. Lett.* **2004**, *93*, 174102.
(9) Vanag, V. K.; Yang, L.; Dolnik, M.; Zhabotinsky, A. M.; Epstein, I. R. Oscillatory Cluster Patterns in a Homogeneous Chemical System with Global Feedback. *Nature* **2000**, *406*, 389–391.
(10) Wang, W.; Kiss, I. Z.; Hudson, J. L. Clustering of Arrays of Chaotic Chemical Oscillators by Feedback and Forcing. *Phys. Rev. Lett.* **2001**, *86*, 4954–4957.
(11) Kuramoto, Y. *Chemical Oscillations, Waves, and Turbulence*; Springer: Berlin, 1984.
(12) Okano, T.; Miyakawa, K. Feedback-Controlled Dynamics in a Two-Dimensional Array of Active Elements. *Phys. Rev. E* **2009**, *80*, 026215.

DOI: 10.1021/jz100238u | *J. Phys. Chem. Lett.* **2010**, *1*, 1241–1246

(13) Taylor, A. F.; Tinsley, M. R.; Wang, F.; Huang, Z. Y.; Showalter, K. Dynamical Quorum Sensing and Synchronization in Large Populations of Chemical Oscillators. *Science* **2009,** *323*, 614–617.
(14) Sivaprakasam, S.; Pierce, I.; Rees, P.; Spencer, P. S.; Shore, K. A.; Valle, A. Inverse Synchronization in Semiconductor Laser Diodes. *Phys. Rev. A* **2001,** *64*, 013805.
(15) Bressloff, P. C.; Coombes, S. Dynamics of Strongly Coupled Spiking Neurons. *Neural Comput.* **2000,** *12*, 91–129.
(16) Rabinovich, M. I.; Varona, P.; Selverston, A. I.; Abarbanel, H. D. I. Dynamical Principles in Neuroscience. *Rev. Mod. Phys.* **2006,** *78*, 1213–1265.
(17) Senthilkumar, D. V.; Kurths, J.; Lakshmanan, M. Inverse Synchronizations in Coupled Time-Delay Systems with Inhibitory Coupling. *Chaos* **2009,** *19*, 023107.
(18) Volkov, E. I.; Ullner, E.; Zaikin, A. A.; Kurths, J. Frequency-Dependent Stochastic Resonance in Inhibitory Coupled Excitable Systems. *Phys. Rev. E* **2003,** *68*, 061112.
(19) Volkov, E. I.; Stolyarov, M. N.; Zaikin, A. A.; Kurths, J. Coherence Resonance and Polymodality in Inhibitory Coupled Excitable Oscillators. *Phys. Rev. E* **2003,** *67*, 066202.
(20) Toiya, M.; Vanag, V. K.; Epstein, I. R. Diffusively Coupled Chemical Oscillators in a Microfluidic Assembly. *Angew. Chem., Int. Ed.* **2008,** *47*, 7753–7755.
(21) Belousov, B. P. A Periodic Reaction and Its Mechanism. In *Collection of Short Papers on Radiation Medicine*; Medgiz: Moscow, 1959; pp 145−152.
(22) Zhabotinsky, A. M. Periodic Liquid Phase Reactions. *Proc. Acad. Sci. USSR* **1964,** *157*, 392–395.
(23) Kaminaga, A.; Vanag, V. K.; Epstein, I. R. "Black Spots" in a Surfactant-Rich BZ-AOT Microemulsion System. *J. Chem. Phys.* **2005,** *122*, 174706.
(24) McIlwaine, R.; Vanag, V. K.; Epstein, I. R. Temperature Control of Pattern Formation in the $Ru(bpy)_3^{2+}$-Catalyzed BZ-AOT System. *Phys. Chem. Chem. Phys.* **2009,** *11*, 1581–1587.
(25) Korshunov, S. E. Phase Transitions in Two-Dimensional Systems with Continuous Degeneracy. *Phys.-Usp.* **2006,** *49*, 225–262.
(26) Miyashita, S.; Shiba, H. Nature of the Phase-Transition of the Two-Dimensional Antiferromagnetic Plane Rotator Model on the Triangular Lattice. *J. Phys. Soc. Jpn.* **1984,** *53*, 1145–1154.
(27) Field, R. J.; Körös, E.; Noyes, R. M. Oscillations in Chemical Systems. II. Thorough Analysis of Temporal Oscillation in Bromate−Cerium−Malonic Acid System. *J. Am. Chem. Soc.* **1972,** *94*, 8649–8664.

DOI: 10.1021/jz100238u | *J. Phys. Chem. Lett.* **2010,** *1*, 1241–1246